Annals of the Academy of Romanian Scientists
Online Edition Physics Series
ISSN 2066 – 8589 Volume 5, Number 1/2015

FINE STRUCTURE OF α-TRANSITIONS WITHIN THE COUPLED CHANNELS FORMALISM

D.S. DELION[1], A. DUMITRESCU[2]

Abstract. *We systematize the available experimental material concerning α-transitions to low-lying excited states in even-even and odd-mass emitters. We show that α-intensities for transitions to excited states depend linearly upon the excitation energy for all known even-even and odd-mass α-emitters. The well known Viola-Seaborg law for α-transitions between ground states can be generalized for transitions to excited states. This rule can be used to predict any α-decay half life to a low-lying excited state. We then describe α-decay transitions to low-lying states in even-even nuclei with $Z > 50$; $N > 82$ by using the coupled channels method. The energy levels and electromagnetic transition rates between the states of the ground band can satisfactorily be reproduced by using two parameters, namely the deformation parameter and the strength of the harmonic Coherent State Model (CSM) Hamiltonian. The B(E2) values can be described in terms of an effective charge which depends linearly on the deformation parameter. The α-emission process is treated by using an α-daughter interaction containing a monopole component, calculated through a double folding procedure with a M3Y interaction plus a repulsive core simulating the Pauli priciple, and a quadrupole-quadrupole (QQ) interaction. The decaying states are identied with the lowest narrow outgoing resonances obtained through the coupled channels method. The α-branching ratios to 2^+ states are reproduced by using the QQ strength. This interaction strength can be fitted with a linear dependence on the deformation parameter, as predicted by CSM. The theoretical intensities to 4^+ and 6^+ states are in reasonable agreement with available experimental data. Predictions are made for spherical, transitional and well deformed even-even α-emitters. Finally we describe electromagnetic and favored α-transitions to rotational bands in odd-mass nuclei built upon a single particle statewith angular momentum projection $\Omega \neq \frac{1}{2}$ in the region $88 \leq Z \leq 98$. We use the particle coupled to an even-even core approach described within CSM and the coupled channels method to estimate partial α-decay widths. We reproduce the energy levels of the rotational band where favored α-transitions occur for 26 nuclei and predict B(E2) values for electromagnetic transitions to the bandhead using a deformation parameter and a Hamiltonian strength parameter for each nucleus, together with an effective collective charge depending linearly on the deformation parameter. Where experimental data is available, the contribution of the single particle effective charge to the total B (E2) value is calculated. The intensity of the transition to the first excited state is reproduced by the QQ coupling strength. It depends linearly both on the nuclear deformation and the square of the reduced width for the decay to the bandhead, respectively. All predicted intensities for transitions to higher excited states are in a reasonable agreement with experimental data.*

Keywords: *α* -emission fine structure, coupled channels method, coherent state model

[1]Prof., ”Horia Hulubei” National Institute of Physics and Nuclear Engineering, 407 Atomistilor, POB MG-6, Bucharest-Magurele, RO-077125, Romania; Academy of Romanian Scientists, 54 Splaiul Independent¸ei, Bucharest, RO-050094, Romania; Bioterra University, 81 Garlei str., Bucharest, RO-013724, Romania; Paper written with financial support of the Romanian Ministry of Education and Research, CNCS UEFISCDI, PN-II-ID-PCE-2011-3-0092, PN-09370102. delion@theory.nipne.ro
2”Horia Hulubei” National Institute of Physics and Nuclear Engineering, 407 Atomistilor, POB MG-6, Bucharest-Magurele, RO-077125, Romania; Department of Physics, University of Bucharest, 405 Atomistilor, POB MG-11, Bucharest-Magurele, RO-077125, Romania

1 Introduction

The phenomenological description of α-decay half-lives uses a simple picture of a preformed α-cluster penetrating through the Coulomb barrier, presented in the works of Gamow [1], Condon and Gurney [2], with a preformation factor proportional to the fragmentation potential, as shown in Ref. [3]. Simple empirical formulas for the half-lives corresponding to ground-to-ground α-transitions have been given in Ref. [4]. The microscopic description needs a more sophisticated R-matrix theory in terms of the formation amplitude, see for instance Refs. [5, 6, 7, 8, 9].

This α-decay spectroscopy was used to investigate the 0^+ and 2^+ excited states in the Pb region [10, 11, 12], and in the U region [13]. α-transitions to excited states, known to constitute the fine structure of the α-decay spectrum, can be analyzed in terms of the hindrance factor (HF), defined by the ratio between formation probabilities to ground and excited states (as defined by Rasmussen [14]). The first estimate of HFs in vibrational nuclei, through the Quasiparticle Random-Phase Approximation (QRPA), was performed in Refs. [15, 16, 17]. Later on, in Ref. [18] was given an explanation for the connection between the HF of the first excited 0^+ state and the neutron number for Pb isotopes in terms of pairing vibrations. More recently, the experimental results concerning the fine structure of 2^+ states were analyzed by using the QRPA formalism [19, 20, 21]. A systematic analysis of α-transitions to 0^+ and 2^+ states in Pb and Po isotopes was performed within the deformed density dependent cluster model, by using a Boltzmann distribution of the preformation factor [22]. In Ref. [23] branching ratios of the α-decay to members of the ground state rotational band and excited 0^+ states in even-even nuclei in the mass regions $180 < A < 202$ and $A \geq 224$ were calculated in the framework of the generalized liquid drop model. Branching ratios and hindrance factors of even-even nuclei in the range $78 \leq Z \leq 102$ were computed in Ref. [24] by using the Coulomb plus proximity potential model for deformed nuclei. The partial half-lives in the Pt-Os region were calculated in Ref. [25] in a semiempirical model, by using the quantum mechanical tunneling mechanism through a Coulomb plus centrifugal plus overlapping potential barrier. The emission of α-particles has become an important tool in the detection of superheavy nuclei, as shown in Ref. [26].

The first calculations of the α-decay widths in rotational nuclei within the coupled channels approach were performed in Ref. [27]. In Ref. [28], HFs were estimated in rotational nuclei by using the Fröman approach [29] for the barrier penetration and a simple phenomenological ansatz for the preformation factor.

The analysis of the α-daughter interaction is a central issue of this field. One of the most popular approaches consists in the double folding procedure, like in Refs. [32, 30, 31]. The double folding potential describing the elastic scattering of α-particles was extended to the medium mass $A \sim 50$-120 nuclei at energies from ~ 13 to 50 MeV in Ref. [33]. In Ref. [34], a systematic fitting procedure was applied to the experimental scattering data of nuclei with $A \sim$ 90-150 at energies around the Coulomb barrier. This was used to obtain local potential parameter sets which have a real folding potential and an imaginary

potential of a Woods-Saxon surface type. In Ref. [35], the potential barrier for α-decay and α-capture was calculated by using partial α-decay half-lives of 344 ground-state-to-ground-state transitions within a liquid drop model including a proximity energy term. Simple expressions were provided for the potential barrier radius and height. A set of parameters for an α-nucleus Woods-Saxon potential was derived in Ref. [36] by using the data for both the α-decay half-lives and the fusion cross sections around the barrier for the reactions $\alpha+^{40}$Ca, $\alpha+^{59}$Co, and $\alpha+^{208}$Pb. The α-decay half-lives were obtained in a cluster model.

The double fine structure of both emitted fragments in the cold fission of ^{252}Cf predicted in Ref. [37] was analyzed in several papers [38, 39, 40]. It turns out that the yields to excited states in both fragments are very sensitive to nuclear structure details such as mean field deformation and density diffusivity. Unfortunately, there is currently very little experimental data in this field, with more data being available regarding the α-decay fine structure in even-even nuclei, see Refs. [41] and [42]. These decays were analyzed within the coupled channels formalism [43, 44], by using the double folding potential plus a repulsive core simulating the Pauli principle, as for cold fission. Several papers were devoted to the coupled channels analysis of the α-decay fine structure [45, 47, 46] using the double folding potential together with the Wildermuth rule to simulate the Pauli principle [48].

In Ref. [49] were analyzed the experimental α-decay half-lives to ground and excited states of nuclei with $222 \leq A \leq 252$ and $88 \leq Z \leq 102$ in a unified penetration model for α-decay and α-capture, by using a Woods-Saxon plus centrifugal plus Coulomb barrier. The evaluated branching ratios for $0^+ \rightarrow 0^+, 2^+, 4^+ \alpha$-transitions in even-even nuclei are in reasonable agreement with the experimental data. A systematic analysis of the α-decay fine structure in odd-odd nuclei in the region $83 \leq Z \leq 101$ was performed in Ref. [50], by using the Coulomb plus proximity potential model for deformed nuclei. More recently, electromagnetic and α-transitions were analyzed within the CSM in Ref. [51] for 40 even-even nuclei with $Z > 82$, $N > 126$.

Several calculations for the fine structure of the emission spectrum have already been made in the case of odd-mass α-emitters. For example, in Ref. [47] a multichannel cluster model together with the coupled channels equation is used to calculate branching ratios to excited states for favored transitions in heavy emitters, in the region $93 < Z < 102$. In Ref. [52], a microscopic method is employed with a Skyrme SLy4 effective interaction. Starting from the Hartree-Fock-Bogoliubov vacuum and quasiparticle excitations, the α-particle formation amplitude is calculated for the α-decay to various channels mostly in the $84 < Z < 88$ region. Several unfavored transitions are treated in this paper and predictions are made for the properties of the g.s.$\rightarrow$g.s. α-trasition in odd-mass superheavy nuclei. The unfavored g.s.$\rightarrow$g.s. α-decay in odd-mass nuclei in the region $64 \leq Z \leq 112$ is also treated in Ref. [53], with the purpose of investigating the effect of the difference in the spin and parity of the ground states on the α-particle and daughter nucleus preformation probability. The calculations are done in the framework of the extended cluster model, with the Wentzel-Kramers-Brillouin penetrability and assault frequency, together with

Table 1: Systematics of α-transitions. Number of studied α-transitions between ground states (g.s.) and from ground to excited states (ex.s.). All experimental data regarding these transitions is taken from http://www.nndc.bnl.gov/ensdf/.

g.s. $\rightarrow$ g.s.	transitions
even-even	149
even-odd	72
odd-even	67
odd-odd	50
total	338
g.s. $\rightarrow$ ex.s.	transitions
even-even	238
favored	130
unfavored	333
total	701

an interaction potential computed on the basis of the Skyrme SLy4 interaction.

The aim of this letter is to review the description of α-transitions to excited states in even-even and odd-mass nuclei in terms of the coupled channel formalism in vibrational, transitional and well deformed α-emitters with $Z > 50$, $N > 82$, by using a unified nuclear structure formalism provided by the CSM.

2 Systematics of α-transitions to excited states

In this Section we review the main features of α-decays to excited states. A statistical overview of the α-transitions is given in Table 1. The experimental data has been taken from the ENSDF database maintained by BNL [54]. Mass and separation energy tables together with related procedures can be investigated in Refs. [55, 56]. We considered in this analysis 338 g.s. to g.s. transitions which fulfiled two conditons:

i) all experimental data that is required in the analysis is available on the ENSDF (total half-life, total alpha-branch, Q-Value, initial and final angular momenta);

ii) a spectroscopic factor for the g.s. to g.s. transition could be calculated in our approach using a fixed set of parameters for all data.

Let us consider the general α-decay transition

$$P(J_P) \rightarrow D(J) + \alpha(L) \ , \tag{2.1}$$

where J_P denotes the spin/parity of the parent nucleus, J the spin/parity of the daughter nucleus and L the angular momentum of the emitted α-particle.

We consider a wave function with a clustered α-daughter ansatz [57] with the total spin of the initial state

$$\Psi_{J_P M_P}(\xi, \mathbf{R}) = \sum_{c=(J,L)} \frac{f_c(R)}{R} \mathcal{Y}^{(c)}_{J_P M_P}(\xi, \hat{R}) \ . \tag{2.2}$$

Here, we introduced the core-angular harmonic

$$\mathcal{Y}^{(c)}_{J_P M_P}(\xi, \hat{R}) = \Big[\Phi_J(\xi) \otimes Y_L(\hat{R})\Big]_{J_P M_P} \ , \tag{2.3}$$

where $\Phi_{JM_J}(\xi)$ denotes the daughter internal wave function with ξ the daughter degrees of freedom, while $Y_{LM_L}(\hat{R})$ is the standard spherical harmonic describing the angular motion of the α-daughter system. The radial function $f_c(R)$ describes the α-daughter radial motion in the channel $c \equiv (J, L)$. At large distances it has an outgoing asymptotic expression

$$f_c(R) \to N_c H^{(+)}_L(\kappa_c R, \chi_c) \ , \tag{2.4}$$

in terms of the Coulomb-Hankel spherical wave depending on the reduced radius $\kappa_c R$ and Coulomb parameter

$$\chi_c = \frac{2Z_D Z_\alpha}{\hbar v_c} \sim \frac{2Z_D Z_\alpha}{\sqrt{Q_\alpha - E_c}} \ , \tag{2.5}$$

where Q_α is the Q-value of the decay process. By using the continuity equation one obtains that the total decay width as a sum of partial widths [57]

$$\begin{aligned} \Gamma &= \sum_c \Gamma_c = \sum_c \hbar v_c \lim_{R\to\infty} |f_c(R)|^2 \\ &= \sum_c \hbar v_c |N_c|^2 \ , \end{aligned} \tag{2.6}$$

where $v_c = \hbar\kappa_c/\mu$ is the center of mass velocity at infinity in the α-daughter channel c.

Each partial width can be formally rewritten in a factorized form at some radius R

$$\Gamma_c = 2\gamma_c^2(R) P_c(R) \ , \tag{2.7}$$

in terms of the so-called squared reduced width and penetrability

$$\begin{aligned} \gamma_c^2(R) &= \frac{\hbar^2}{2\mu R} |f_c(r)|^2 \\ P_c(R) &= \frac{\kappa_c R}{\left|H^{(+)}_L(\kappa_c R, \chi_c)\right|^2} . \end{aligned} \tag{2.8}$$

The product does not depend upon the radius, but this representation allows us to estimate the decay width by using the wave function on the nuclear surface.

The simplest case is the emission between even-even nuclei from the ground state of the parent nucleus with $J_P = 0$. The angular momentum of the α-particle coincides with the daughter spin $J = L$ and the core-angular harmonic is given by

$$\mathcal{Y}_0^{(c)}(\xi_D, \hat{R}) \ , \quad c = J \ . \tag{2.9}$$

In particular in Ref. [43] the ground band is described by a rigid rotator, while in Ref. [58] it is generalized by using a projected coherent state depending on the deformation parameter. For small values of this parameter one obtains a vibrational spectrum, while for large values a rotational one is found.

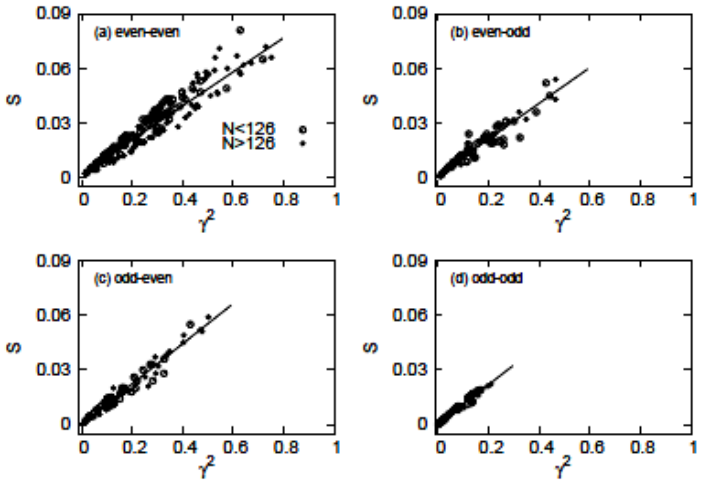

Figure 1: Spectroscopic factor versus the α-formation probability for even-even (a), even-odd (b), odd-even (c) and odd-odd emitters (d).

For transitions from odd-mass nuclei, if the state of the unpaired nucleon remains unchanged during the decay process, then the transition is known as favored, otherwise it is called unfavored. In this case the wave function of the daughter nucleus is given by a particle-core ansatz

$$\Phi_{JM_J}(\xi, \mathbf{r}) = \sum_J X_J^{(J_D)} \left[\varphi_{J_D}(\xi) \otimes \psi_{j_D}(\mathbf{r})\right]_{JM_J} \ , \tag{2.10}$$

where $\varphi_{J_D}(\xi)$ is the wave function of the even-even core and $\psi_{j_D m_D}(\mathbf{r})$ is the single-particle orbital. The mixing coefficients are found by diagonalizing a quadrupole-quadrupole interaction between the even-even core and the odd particle. A more general ansatz assumes a quasiparticle-core coupling. Such a model describes bands built on top of single particle states. In odd-odd nuclei the single-particle orbital is replaced by a proton-neutron wave function.

Let us mention that for some odd-mass nuclei around ^{208}Pb two quasiparticles can be broken, being coupled to some angular momentum J_{pair}=2,4,6,...

. Thus, one can use the three quasiparticle-core model [59]. In our analysis we considered only α-transitions in odd-mass nuclei between nuclei described by Eq. (2.10).

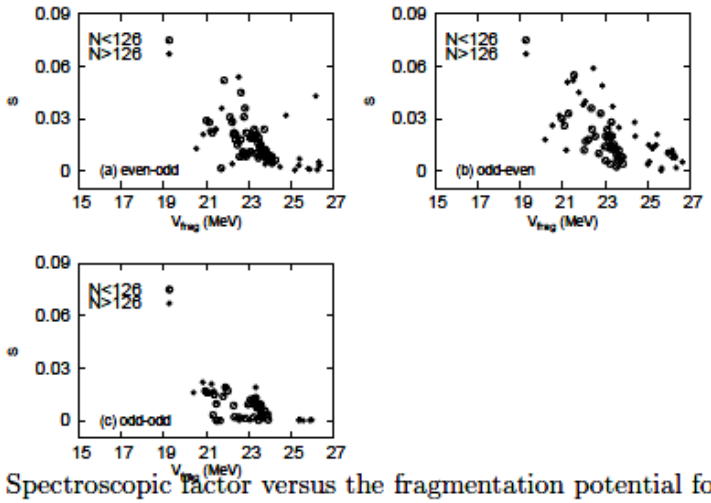

Figure 2: Spectroscopic factor versus the fragmentation potential for even-odd (a), odd-even (b) and odd-odd emitters (c).

The most popular α-daughter potential is given by the double folding integration method of the nucleon-nucleon interaction with density distributions of the emitted fragments. A potential determined from α-scattering experiments is used for the nucleon-nucleon interaction, thus assuming that the α-particle exists with a probability equal to unity. Actually, the particle forms with a probability given by the spectroscopic factor

$$S = \frac{\Gamma_{exp}}{\Gamma_{th}} = \frac{T_{th}}{T_{exp}} \ , \tag{2.11}$$

which is less than unity. Eq. (2.7) can be interpreted as a product between the α-formation probability γ^2 and the probability P of the penetration through the Coulomb barrier. Therefore the spectroscopic factor S and α-formation probability are proportional.

In Ref. [3] it has been shown analitically that the logarithm of the reduced decay width is proportional to the fragmentation potential

$$V_{frag} = V_C - (Q_\alpha - E_J). \tag{2.12}$$

$V_C(R_B)$ is the Coulomb barrier and E_J the excitation energy in the daughter nucleus. In Ref. [3] this correlation was evidenced for even-even emitters. A similar picture holds for even-odd nuclei, as can be seen from Fig. 2 (a), as well as for odd-even (b) and odd-odd emitters (c).

As a direct consequence of this law is the linear dependence between the

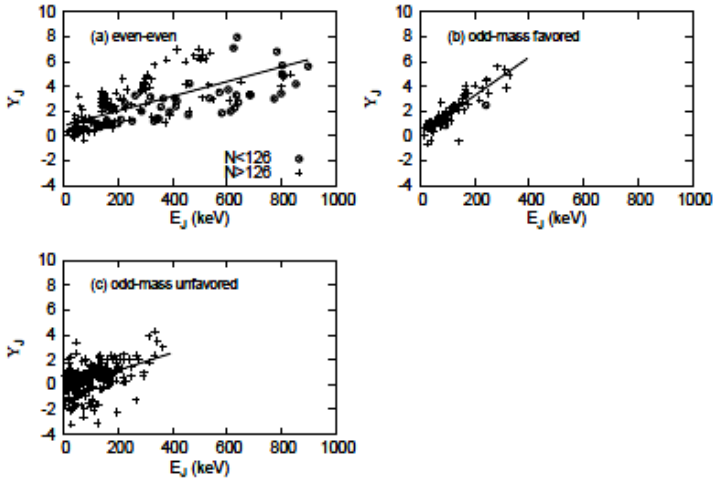

Figure 3: Intensity Υ_J versus the excitation energy in the daughter nucleus E_J, $1 \leq J \leq 6$, in even-even nuclei (a), for odd-mass favored (b) and unfavored transitions (c).

intensity of the ground to excited state transition and the excitation energy [58]

$$\Upsilon_J \equiv \log_{10} \frac{\Gamma_0}{\Gamma_J} = gE_J + h \ . \tag{2.13}$$

This correlation with a positive slope is clearly evidenced for even-even emitters in Fig. 3 (a). A similar correlation remains valid for odd-mass emitters. This feature is evidenced in Fig. 3 (b) for favored transitions to excited states of rotational bands and in Fig. 3 (c) for unfavored transitions to excited states of rotational bands.

The most popular systematics for α-transitions between ground states is given by the Viola-Seaborg rule [60], where the logarithm of the total half life depends on the Coulomb parameter and charge number of the daughter nucleus. It was used to describe transitions between ground states in the case of α-decay [61], as well as proton [62] and heavy-cluster emission [63]. Other simple formulas for α-emission have been provided in Refs. [64, 65]. The Viola-Seaborg rule is a direct consequence of two facts, namely the exponential dependence of the penetrability upon the Coulomb parameter and the dependence of the squared reduced width upon the charge number, given by the fragmentation potential in Eq. (2.12). Due to the fact that the channel Coulomb parameter (2.5) depends on the excitation energy of the daughter nucleus, this rule can be generalized for partial half-lives of transitions to excited states

$$\log_{10} T_J \ = \ \frac{aZ_D + b}{\sqrt{Q_\alpha - E_J}} + cZ_D + d \equiv V_J \ . \tag{2.14}$$

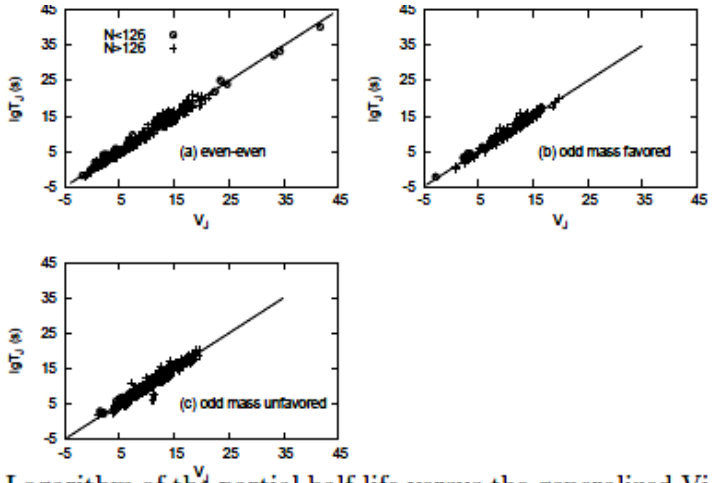

Figure 4: Logarithm of the partial half-life versus the generalized Viola-Seaborg parameter (3.64) for even-even (a), odd-mass favored (b) and odd-mass unfavored emitters (c). Here we considered data with $1 \leq J \leq 6$ in daughter nuclei.

This generalized Viola-Seaborg law is very well satisfied by all available experimental data concerning transitions to excited states with $1 \leq J \leq 6$, as can be seen for even-even emitters in Fig. 4 (a), as well as for odd-mass emitters in favored (b) and unfavored transitions (c). We notice that one obtains similar values of the parameters both for even-even and odd-mass emitters, in the case of favored as well as unfavored transitions.

3 Theoretical background

In this Section we describe the structure of even-even and odd-mass nuclei in terms of the Coherent State Model (CSM) and we describe α-decay widths by using the coupled channels method.

3.1 Coherent State Model for even-even nuclei

The CSM was proposed in Refs. [66, 67] as a tool to describe in a unified way the spectra of vibrational, transitional and rotational nuclei. It treats the surface vibrations of a deformed nucleus by using an exponential superposition of boson operators [68, 69]. The model was later extensively developed in Refs. [70, 71] for the description of low-lying as well as high spin states in nuclei, including isospin degrees of freedom (for a review, see Ref. [72]).

The wave function of an axially deformed even-even nucleus in its intrinsic system of coordinates is given by a coherent superposition of quadrupole boson operators $b_{2\mu}$ with $\mu = 0$ acting on the vacuum state

$$|\psi_g\rangle = e^{d\left(b_{20}^{\dagger} - b_{20}\right)}|0\rangle \ , \tag{3.1}$$

in terms of the deformation parameter proportional to the static quadrupole deformation [70]

$$d = \kappa\beta_2 \ . \tag{3.2}$$

Physical states which define the ground band are obtained by projecting out the angular momentum

$$|\varphi_J^{(g)}\rangle = \mathcal{N}_J^{(g)} \hat{P}_{M0}^J |\psi_g\rangle \ , \tag{3.3}$$

in terms of the projection operator

$$\hat{P}_{MK}^J = \sqrt{\frac{2J+1}{8\pi^2}} \int \mathrm{d}\omega D_{MK}^J(\omega) \hat{R}(\omega), \tag{3.4}$$

where $D_{MK}^J(\omega)$ is a Wigner function and $\hat{R}(\omega)$ is a rotation operator, parametrized by the Euler angles ω.

The norm of the wave function is given by [71]

$$\mathcal{N}_J^{(g)} = \left[(2J+1) I_J^{(0)}(d)\right]^{-1/2} e^{d^2/2} \ , \tag{3.5}$$

in terms of the following integral

$$I_J^{(0)}(d) = \int_0^1 P_J(x) e^{d^2 P_2(x)} dx \ , \tag{3.6}$$

where $P_J(x)$ are Legendre polynomials. The simplest estimate of the ground band energy spectrum is given by

$$\begin{aligned} E_J(d) &= A_1 \left[\langle\varphi_J^{(g)}|\hat{N}|\varphi_J^{(g)}\rangle - \langle\varphi_0^{(g)}|\hat{N}|\varphi_0^{(g)}\rangle\right] \\ &= A_1 d^2 \left[\mathcal{I}_J(d) - \mathcal{I}_0(d)\right] \ , \end{aligned} \tag{3.7}$$

where $\hat{N}$ is the operator for the number of bosons. Here, we defined the following function depending on the deformation parameter

$$\begin{aligned} \mathcal{I}_J(d) &= \frac{I_J^{(1)}(d)}{I_J^{(0)}(d)} \\ I_J^{(1)}(d) &\equiv \frac{dI_J^{(0)}(x)}{dx}, \quad x = d^2 \ . \end{aligned} \tag{3.8}$$

Notice that for small values of d the energy spectrum has a vibrational character $E_J \sim A_1 J$, while for large values it has a rotational shape $E_J \sim A_1 J(J+1)$ [66]. A one parameter description of the CSM Hamiltonian leads to a universal dependence of the energy ratio on the deformation parameter

$$\frac{E_{J+2}}{E_J} = \frac{\mathcal{I}_{J+2}(d) - \mathcal{I}_0(d)}{\mathcal{I}_J(d) - \mathcal{I}_0(d)} \ . \tag{3.9}$$

3.2 Electromagnetic transitions in even-even nuclei

The B(E2) value for electromagnetic transitions connecting ground band states is given by [71]

$$\begin{aligned} B(E2: J' \to J) &= \left[\frac{1}{\hat{J}'}\langle\varphi_J^{(g)}||T_2||\varphi_{J'}^{(g)}\rangle\right]^2 \\ &= \left[q_{eff}\langle J'0;20|J0\rangle d\left(\frac{\hat{J}'\mathcal{N}_{J'}^{(g)}}{\hat{J}\mathcal{N}_J^{(g)}}+\frac{\hat{J}\mathcal{N}_J^{(g)}}{\hat{J}'\mathcal{N}_{J'}^{(g)}}\right)\right]^2 , \end{aligned} \tag{3.10}$$

in terms of the effective charge depending linearly on the deformation parameter

$$q_{eff} = q_0\left(1-\sqrt{\frac{2}{7}}a_q d\right) , \tag{3.11}$$

and of the quadrupole transition operator with harmonic and anharmonic terms

$$\begin{aligned} T_{2\mu} &= q_0 Q_{2\mu} \\ Q_{2\mu} &= b_{2\mu}^\dagger + \tilde{b}_{2\mu} + a_q\left[\left(b_2^\dagger\otimes b_2^\dagger\right)_{2\mu} + (b_2\otimes b_2)_{2\mu}\right] , \end{aligned} \tag{3.12}$$

where q_0 is the charge parameter, a_q the anharmonic strength and $\tilde{b}_{2\mu} = b_{2-\mu}(-)^\mu$. Here, $\hat{J} = \sqrt{2J+1}$ and the braket stands for the standard Clebsch-Gordan coefficient.

The reduced matrix element is defined in the usual convention

$$\langle JM|T_{\lambda\mu}|J'M'\rangle = \frac{\langle J'M';\lambda\mu|JM\rangle}{\hat{J}}\langle J||T_\lambda||J'\rangle . \tag{3.13}$$

The excitation energy of the $J = 2$ state, given by Eq. (3.7), can be connected to the B(E2;2→0) value of Eq. (3.10) as follows:

$$\frac{E_2}{A_1} = \frac{7}{2d}\frac{(I_2^{(1)}I_0^{(0)} - I_0^{(1)}I_2^{(0)})}{(5I_0^{(0)}+I_2^{(0)})^2}\frac{B(E2;2\to 0)}{q_{eff}^2} . \tag{3.14}$$

3.3 Nucleon coupled to a coherent state core

For an odd-mass nucleus, the state of total angular momentum I and projection M is given by projecting out the product between the coherent state (3.1) and the single particle state ψ_{jm}, where j is a shorthand notation for all of the quantum numbers of the state, that is

$$\Phi_{IM} = P_{M0}^I\left[\psi_j\phi_g\right] . \tag{3.15}$$

A straighforward calculation leads to the following result

$$\Phi_{IM} = \sum_J X_I^{Jj}\left[\varphi_J^{(g)}\otimes\psi_{jm}\right]_{IM} , \tag{3.16}$$

with normalization coefficients X_I^{Jj} given by

$$X_I^{Jj} = \frac{\left(\mathcal{N}_J^{(g)}\right)^{-1} \langle jJ;\Omega 0|I\Omega\rangle}{\sqrt{\sum_{J'}\left(\mathcal{N}_{J'}^{(g)}\right)^{-2}\left(\langle jJ'\Omega 0|I\Omega\rangle\right)^2}}, \tag{3.17}$$

where Ω is the fixed z-projection of the single-particle angular momentum j. More details on this procedure can be consulted in Ref. [73].

The states built upon the bandhead $I = j = \Omega$ that follow the sequence $I = \Omega, \Omega+1, \Omega+2, \ldots$ constitute a rotational band. In the Nilsson model, these states are labeled by the set $\Omega^\pi\,[Nn_z\Lambda]$, where π is the parity, N is the principal quantum number, n_z the number of nodes of the radial wavefunction in the z direction and Λ the projection of the single-particle orbital angular momentum. The last three numbers act only as labels, as the good quantum numbers are only Ω and π.

The simplest Hamiltonian that can describe such a rotational structure consists of two terms [73]:

$$H = A_1 b_2^\dagger \cdot b_2 - A_2 r^2 \left(b_2^\dagger + \tilde{b}_2\right) \cdot Y_2. \tag{3.18}$$

where by dot we denoted the scalar product. A_1 is a strength parameter required to fit experimental data and A_2 is the strength of the particle-core QQ interaction.

For the description of the rotational band the only relevant parameter is A_1 due to the fact that the particle-core term is common. Instead of solving the eigenvalue problem by a full diagonalization procedure, a simpler approach, involving the analytical expression for the diagonal matrix elements of the Hamiltonian (3.18) in the basis of Eq. (3.16) suffices:

$$\begin{aligned}\langle IM|H|IM\rangle &= A_1 d^2 f_{j\Omega I} - d\left(N+\frac{3}{2}\right)\times \\ &\times \langle j2;\Omega 0|j\Omega\rangle\langle j2;\frac{1}{2}0|j\frac{1}{2}\rangle,\end{aligned} \tag{3.19}$$

with $f_{j\Omega I}$ given by

$$f_{j\Omega I} = \frac{\sum_J \langle Ij;\Omega-\Omega|J0\rangle^2 \mathcal{I}_J^{(1)}(d)}{\sum_J \langle Ij;\Omega-\Omega|J0\rangle^2 \mathcal{I}_J^{(0)}(d)}\,. \tag{3.20}$$

The shape of such a spectrum is dependent both on the deformation parameter and on the value of Ω, as can be seen in Fig. 5.

While this approach is adequate, if a greater precision in the description of the nuclear energy spectrum is required, then more terms can be added to the Hamiltonian (3.18), as shown in Ref. [73]. Let us also mention that the

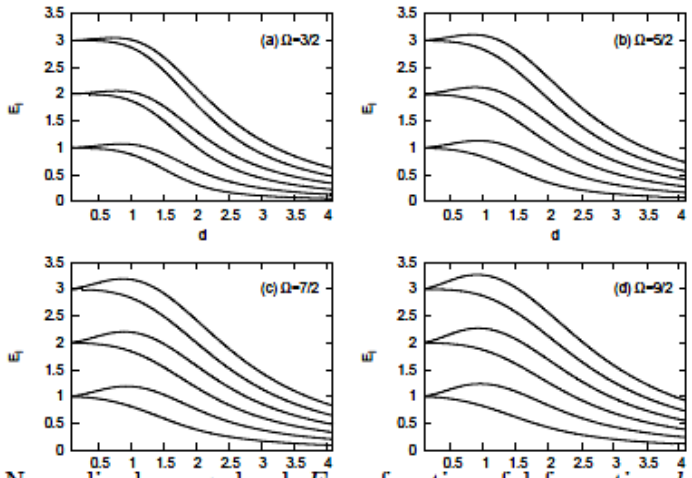

Figure 5: Normalized energy levels E_I as function of deformation d, for different values of the single particle angular momentum projection Ω.

development presented here and expanded upon in Ref. [73] is appropriate for any rotational band built upon an angular momentum projection $\Omega \neq \frac{1}{2}$. The special case $\Omega = \frac{1}{2}$ requires a modification of the formalism.

3.4 Electromagnetic transitions in odd-mass nuclei

The $B\,(E2)$ values of electric quadrupole transitions follow from both collective and single particle contributions

$$\begin{aligned} B\,(E2; I_2 \to I_1) &= [\frac{1}{\hat{I}_2}\langle I_1||q_0^c Q_2^c||I_2\rangle + \\ &+ \frac{1}{\hat{I}_2}\langle I_1||q_0^{sp} Q_2^{sp}||I_2\rangle)]^2, \end{aligned} \tag{3.21}$$

where q_0^c and q_0^{sp} are effective charges.

The collective quadrupole transition operator has both harmonic and anharmonic contributions

$$Q_{2\mu}^c = b_{2\mu}^\dagger + \tilde{b}_{2\mu} + a_q \left[\left(b_2^\dagger \otimes b_2^\dagger\right)_{2\mu} + (b_2 \otimes b_2)_{2\mu}\right], \tag{3.22}$$

with a_q the anharmonic strength. Its reduced matrix elements on the states of the core are

$$\begin{aligned} \langle \varphi_{J_1}^{(g)}||q_0^c Q_2^c||\varphi_{J_2}^{(g)}\rangle &= \frac{q_{eff} d}{\hat{J}_2 \mathcal{N}_{J_1}^{(g)} \mathcal{N}_{J_2}^{(g)}} \langle J_1 2; 00|J_2 0\rangle \times \\ &\times \left[\hat{J}_1^2 \left(\mathcal{N}_{J_1}^{(g)}\right)^2 + \hat{J}_2^2 \left(\mathcal{N}_{J_2}^{(g)}\right)^2\right], \end{aligned} \tag{3.23}$$

with q_{eff} given by a linear formula in d

$$q_{eff} = q_0^c \left(1 - \sqrt{\frac{2}{7}} a_q d \right) . \tag{3.24}$$

The single particle quadrupole transition operator has the occupation number representation

$$Q_{2\mu}^{sp} = \sum_{j_1 j_2} \frac{1}{\hat{2}} \langle j_1 || r^2 Y_2 || j_2 \rangle \left(c_{j_1}^\dagger \tilde{c}_{j_2} \right)_{2\mu} . \tag{3.25}$$

Explicit expressions for the matrix elements of these operators over the states of the odd-mass nucleus follow from the above results and the use of standard angular momentum algebra. For our particular case of fixed j, the final formulas are

$$\begin{aligned} \langle I_1 || q_0^c Q_2^c || I_2 \rangle &= \sum_{J_1 J_2} X_{I_1}^{J_1 j} X_{I_2}^{J_2 j} \hat{I}_1 \hat{I}_2 (-)^{j - I_1} \times \\ &\times \mathcal{W}(I_1 J_1 I_2 J_2; j2) \langle \varphi_{J_1}^{(g)} || q_0^c Q_2^c || \varphi_{J_2}^{(g)} \rangle , \end{aligned} \tag{3.26}$$

$$\begin{aligned} \langle I_1 || q_0^{sp} Q_2^{sp} || I_2 \rangle &= \sum_{J_1} X_{I_1}^{J_1 j} X_{I_2}^{J_1 j} \hat{I}_1 \hat{I}_2 (-)^{j + I_2} \times \\ &\times \mathcal{W}(I_1 j I_2 j; J_1 2) \langle j || q_0^{sp} r^2 Y_2 || j \rangle , \end{aligned} \tag{3.27}$$

with $\mathcal{W}$ a Racah coefficient.

3.5 Coupled channels approach to α-emission for even-even emitters

Let us consider an α-decay process connecting the ground state to an excited level

$$P \to D(J) + \alpha \ , \tag{3.28}$$

where J denotes the spin of the excited level in the even-even axially deformed daughter nucleus. The wave function of the α-daughter system has the total spin of the ground state (i.e. zero)

$$\begin{aligned} \Psi(b_2, \mathbf{R}) &= \sum_J \frac{f_J(R)}{R} \mathcal{Z}_J(b_2, \Omega) \\ \mathcal{Z}_J(b_2, \Omega) &\equiv \left[\varphi_J^{(g)}(b_2) \otimes Y_J(\Omega) \right]_0 , \end{aligned} \tag{3.29}$$

where $\mathbf{R} \equiv (R, \Omega)$ denotes the distance between the centers of the two fragments. We describe the α-daughter dynamics by using the stationary Schrödinger equation, i.e.

$$H \Psi(b_2, \mathbf{R}) = Q_\alpha \Psi(b_2, \mathbf{R}) \ , \tag{3.30}$$

where Q_α is the Q-value of the decay process. The Hamiltonian

$$H = -\frac{\hbar^2}{2\mu}\nabla_R^2 + H_D(b_2) + V(b_2, \mathbf{R}) \ . \tag{3.31}$$

contains the kinetic operator, depending on the reduced mass

$$\mu = m_N \frac{4A_D}{4 + A_D} \ , \tag{3.32}$$

a term describing the dynamics of the nuclear core $H_D(b_2)$ and the α-core interaction

$$V(b_2, \mathbf{R}) = V_0(R) + V_2(b_2, \mathbf{R}) \ . \tag{3.33}$$

The monopole part of the interaction is given by a pocket-like shape [43]

$$\begin{aligned} V_0(R) &= v_a \overline{V}_0(R), \quad R > R_m \\ &= c(R - R_{min})^2 - v_0, \quad R \leq R_m \ , \end{aligned} \tag{3.34}$$

where $\overline{V}_0$ is the Coulomb plus nuclear potential, estimated by using the double folding procedure of the M3Y particle-particle interaction with Reid soft core parametrisation [74, 75, 76] (see [57] for computational details).

The parameters of the nuclear interaction between the α-particle and daughter nucleus defining $\overline{V}_0$ were determined by using scattering experiments which assumed that the α-particle exists with certainty, that is $v_a = 1$. Therefore the interaction should be multiplied by a factor $v_a < 1$, which simulates the formation of the cluster on the nuclear surface. The value of v_a is fixed by the absolute value of the total decay width [44]. It is important to emphasize that α-decay branching ratios to members of the ground band have a weak dependence of this factor [43]. Another possibility is to leave the interaction potential unquenched and to consider the spectroscopic factor

$$S = \frac{\Gamma_{expt}}{\Gamma_{theor}}, \tag{3.35}$$

as a measure of the particle formation probability, as in Ref. [79].

The second line of Eq. (3.34) is the repulsive core simulating the Pauli principle, namely the fact that the α-particle can exist only on the nuclear surface [3]. This core also fixes the energy of the first resonant state to the experimental Q-value Q_α.

We applied the procedure of Ref. [43] to determine the matching radius R_m and the coordinate R_{min}, corresponding to the minimal value v_0, by using the equality between the external attractive potential and internal repulsion, together with their derivatives. Therefore, the above interaction is continuous and it depends on the repulsive strength c and the potential depth v_0 [43]. We considered a given value for c and fixed v_0 by the Q-value of the α-decay process.

The $\lambda=2$ term is given by the quadrupole-quadrupole (QQ) interaction

$$V_2(b_2,\mathbf{R}) = -C_0(R-R_{min})\frac{dV_0(R)}{dR}\sqrt{5}\left[Q_2\otimes Y_2(\Omega)\right]_0 . \quad (3.36)$$

By using the orthonormality of the angular functions entering the superposition (3.29), one obtains in a standard way the coupled system of differential equations for radial components [57]

$$\frac{d^2f_J(R)}{d\rho_J^2}=\sum_{J'}A_{JJ'}(R)f_{J'}(R) , \quad (3.37)$$

where the coupling matrix is given by

$$\begin{aligned} A_{JJ'}(R) &= \left[\frac{J(J+1)}{\rho_J^2}+\frac{V_0(R)}{Q_\alpha-E_J}-1\right]\delta_{JJ'} \\ &+ \frac{1}{Q_\alpha-E_J}\langle\mathcal{Z}_J|V_2(b_2,\mathbf{R})|\mathcal{Z}_{J'}\rangle , \end{aligned} \quad (3.38)$$

in terms of the reduced radius

$$\rho_J = \kappa_J R, \quad \kappa_J=\sqrt{\frac{2\mu(Q_\alpha-E_J)}{\hbar^2}} . \quad (3.39)$$

The matrix element of the α-core coupling entering Eq. (3.38) is proportional to the reduced matrix element defining electromagnetic transitions (3.10), but with a different anharmonic parameter [66]

$$\begin{aligned} \langle\mathcal{Z}_J|V_2(b_2,\mathbf{R})|\mathcal{Z}_{J'}\rangle &= -C_0(R-R_{min})\frac{dV_0(R)}{dR}\frac{1}{\hat{2}\hat{J}\hat{J}'} \\ &\times \langle\varphi_J^{(g)}||Q_2||\varphi_{J'}^{(g)}\rangle\langle Y_J||Y_2||Y_{J'}\rangle \\ &= -C\left(R-R_{min}\right)\frac{dV_0(R)}{dR}\frac{d}{\sqrt{4\pi}}\frac{\hat{J}}{\hat{J}'} \\ &\times \langle J0;20|J'0\rangle^2\left(\frac{\hat{J}'\mathcal{N}_{J'}^{(g)}}{\hat{J}\mathcal{N}_J^{(g)}}+\frac{\hat{J}\mathcal{N}_J^{(g)}}{\hat{J}'\mathcal{N}_{J'}^{(g)}}\right) , \end{aligned} \quad (3.40)$$

where we defined the effective α-daughter coupling strength

$$C=C_0\left(1-\sqrt{\frac{2}{7}}a_\alpha d\right) . \quad (3.41)$$

3.6 Favored α-emission in the coupled channels approach for odd-mass emitters

The decay phenomenon of interest connects the ground state of the parent nucleus of angular momentum I_P to an excited state of angular momentum I

of the daughter and an α-particle of angular momentum l, in such a way that the total angular momentum I_P is conserved

$$P\left(I_P\right) \rightarrow D\left(I\right) + \alpha\left(l\right). \tag{3.42}$$

An important remark is that both the initial state of the parent and the final state of the daughter are built upon the same single particle orbital j. This is known as a favored α-transition, due to the fact that it usually has a large branching ratio. The situation where the initial and final single particle orbitals are different is known as an unfavored α-transition. For the favored case, the transition from the ground state to the bandhead built atop the j orbital in the daughter nucleus generally has the highest decay width, and transitions on excited states of the band form the fine structure of the spectrum.

The total wavefunction of the α-daughter system can be assumed to be separable in radial and angular parts and expanded in the angular momentum basis

$$\Psi\left(b_2^{\dagger}, \mathbf{R}\right) = \sum_{Il} \frac{f_{Il}\left(R\right)}{R} \mathcal{Z}_{Il}\left(b_2^{\dagger}, \omega\right), \tag{3.43}$$

where the angular components are given by the coupling to good angular momentum between a wave function for the odd-mass daughter nucleus and a spherical harmonic for the α-particle

$$\mathcal{Z}_{Il}\left(b_2^{\dagger}, \omega\right) = \left[\Phi_{IM}\left(b_2^{\dagger}\right) \otimes Y_{lm}\left(\omega\right)\right]_{I_P M_P}. \tag{3.44}$$

Here, $\mathbf{R} = (R, \omega)$ is the relative vector between the two fragments. Each pair of angular momentum values defines a decay channel

$$(I, l) = c. \tag{3.45}$$

The function Ψ must satisfy the stationary Schrödinger equation (3.30), where the Hamiltonian is given by (3.31) containing the potential energy (3.33). The α-core part is given by the QQ interaction (3.36). The angular functions entering the expansion of Eq. (3.43) are orthonormal. Using this, one obtains in a standard way the system of coupled differential equations for radial components

$$\frac{d^2 f_{I_1 l_1}\left(R\right)}{d\rho_{I_1}^2} = \sum_{I_2 l_2} A_{I_1 l_1; I_2 l_2}\left(R\right) f_{I_2 l_2}\left(R\right), \tag{3.46}$$

with the coupling matrix having the expression

$$\begin{aligned} A_{I_1 l_1; I_2 l_2}\left(R\right) &= \left[\frac{l_1\left(l_1+1\right)}{\rho_{I_1}^2} + \frac{V_0\left(R\right)}{Q_\alpha - E_{I_1}} - 1\right] \delta_{I_1 l_1; I_2 l_2} + \\ &+ \frac{1}{Q_\alpha - E_{I_1}} \langle \mathcal{Z}_{I_1 l_1} | V_2\left(b_2^{\dagger}, \mathbf{R}\right) | \mathcal{Z}_{I_2 l_2} \rangle, \end{aligned} \tag{3.47}$$

in terms of the reduced radius

$$\rho_I = \kappa_I R,\ \kappa_I = \sqrt{\frac{2\mu\left(Q_\alpha - E_I\right)}{\hbar^2}}. \tag{3.48}$$

Notice that κ_I has the same value for all the channels of fixed I, so the supplementary l-index can be omitted both for the wave number and reduced radius.

The coupling term of the matrix is found by the same method as in the previous section to be

$$\begin{aligned}\langle \mathcal{Z}_{I_1 l_1}|V_2\left(b_2^\dagger,\mathbf{R}\right)|\mathcal{Z}_{I_2 l_2}\rangle &= \sum_{J_1 J_2} X_{I_1}^{J_1 j} X_{I_2}^{J_2 j}\langle\varphi_{J_1}^{(g)}||Q_2^c||\varphi_{J_2}^{(g)}\rangle \\ &\times \langle l_1||Y_2||l_2\rangle \hat{I}_P^2 \hat{I}_1 \hat{I}_2 \hat{j}\,(-)^{I_2-I_P+l_2} \\ &\times \mathcal{W}(I_1 l_1 I_2 l_2; I_P 2)\begin{Bmatrix} J_1 & I_1 & j \\ J_2 & I_2 & j \\ 2 & 2 & 0 \end{Bmatrix}\end{aligned} \tag{3.49}$$

where the curly brackets denote a 9j-symbol. Since the reduced matrix element between the states of the core is a linear function of the deformation [71], one can express this linearity in terms of an effective α-nucleus coupling strength given by Eq. (3.41).

3.7 Resonant states

A state decaying by α-emission is identified with a narrow resonant solution of the system of equations (3.37), containing only outgoing components. In order to solve this system of equations we first define the internal and external fundamental solutions which satisfy the boundary conditions

$$\begin{aligned}\mathcal{R}_{JI}(R) &\overset{R\to 0}{\longrightarrow} \delta_{JI}\varepsilon_J\ , \\ \mathcal{H}_{JI}^{(+)}(R) \equiv \mathcal{G}_{JI}(R) + i\mathcal{F}_{JI}(R) &\overset{R\to\infty}{\longrightarrow} \delta_{JI} H_J^{(+)}(\kappa_J R) \equiv \delta_{JI} \times \\ &\times \left[G_J(\kappa_J R) + iF_J(\kappa_J R)\right]\ ,\end{aligned} \tag{3.50}$$

where ε_J are arbitrary small numbers. Here, the index J labels the component and I the solution, $G_J(\kappa_J R)$ and $F_J(\kappa_J R)$ are the standard irregular and regular spherical Coulomb functions, depending on the momentum κ_J in the channel J, defined by Eq. (3.39).

Each component of the solution is built as a superposition of N independent fundamental solutions. We impose the matching conditions at some radius R_1 inside the barrier and obtain

$$\begin{aligned} f_J(R_1) &= \sum_I \mathcal{R}_{JI}(R_1) M_I = \sum_I \mathcal{H}_{JI}^{(+)}(R_1) N_I \\ \frac{df_J(R_1)}{dR} &= \sum_I \frac{d\mathcal{R}_{JI}(R_1)}{dR} M_I = \sum_I \frac{d\mathcal{H}_{JI}^{(+)}(R_1)}{dR} N_I\ , \end{aligned} \tag{3.51}$$

where N_I are called scattering amplitudes. One thus arrives at the following secular equation

$$\begin{vmatrix} \mathcal{R}(R_1) & \mathcal{H}^{(+)}(R_1) \\ \frac{d\mathcal{R}(R_1)}{dR} & \frac{d\mathcal{H}^{(+)}(R_1)}{dR} \end{vmatrix} \approx \begin{vmatrix} \mathcal{R}(R_1) & \mathcal{G}(R_1) \\ \frac{d\mathcal{R}(R_1)}{dR} & \frac{d\mathcal{G}(R_1)}{dR} \end{vmatrix} = 0 \ . \tag{3.52}$$

The first condition is fulfilled for the complex energies of the resonant states. They practically coincide with the real scattering resonant states, due to the fact that the imaginary parts of energies are much smaller than the corresponding real parts, which implies vanishing regular Coulomb functions F_J inside the barrier. The roots of the equation (3.52) do not depend upon the matching radius R_1, because both internal and external solutions satisfy the same Schrödinger equation. The unknown coefficients M_I and N_I are obtained from the normalisation of the wave function in the internal region

$$\sum_J \int_{R_0}^{R_2} |f_J(R)|^2 dR = 1 \ , \tag{3.53}$$

where R_2 is the external turning point.

3.8 α-decay observables

We will use the CSM deformation parameter d to determine the α-decay fine structure by calculating the logarithm of the ratio between decay widths to ground and J^+ states, i.e.

$$\Upsilon_J \equiv \log_{10} \frac{\Gamma_0}{\Gamma_J} \ , \tag{3.54}$$

where partial widths are given by the rule [57]

$$\Gamma \ = \ \sum_J \Gamma_J = \sum_J \hbar v_J \lim_{R\to\infty} |f_J(R)|^2 = \sum_J \hbar v_J |N_J|^2 \ , \tag{3.55}$$

with Γ the total decay width and v_J the center of mass velocity at infinity in channel J, i.e.

$$v_J = \frac{\hbar \kappa_J}{\mu} \ . \tag{3.56}$$

We call the quantity Υ_J the intensity of the α-decay to the J-th state [43]. The total half-life is related to the decay width through the formula

$$T = \frac{\hbar \ln 2}{\Gamma} \ . \tag{3.57}$$

In order to extract the influence of the Coulomb barrier one defines the logarithm of the HF

$$\log_{10} HF_J \equiv \log_{10} \frac{\gamma_0^2}{\gamma_J^2} = I_J - \log_{10} \frac{P_0}{P_J} \ , \tag{3.58}$$

where the square of the reduced width (or preformation probability) is defined by the standard factorisation [57]

$$\Gamma_J = 2P_J(R)\gamma_J^2(R) \ , \tag{3.59}$$

in terms of the Coulomb penetrability

$$P_J(R) = \frac{\kappa_J R}{F_J^2(\kappa_J R) + G_J^2(\kappa_J R)} \approx \frac{\kappa_J R}{G_J^2(\kappa_J R)} \ , \tag{3.60}$$

computed at the touching radius

$$R = 1.2(4^{1/3} + A_D^{1/3}) \ , \tag{3.61}$$

where A_D is the mass number of the daughter nucleus.

Let us mention that the logarithm of the penetrability depends linearly upon the Coulomb parameter

$$log_{10}P_J \sim \chi_J = \frac{4Z_D}{\hbar v_J} \sim \frac{Z_D}{\sqrt{Q_\alpha - E_J}} \ . \tag{3.62}$$

By fitting the realistic pocket-like potential (3.34) to a shifted harmonic oscillator with frequency ω, matched to the Coulomb barrier at the radius r_B, one obtains the universal law for reduced widths [3]

$$\log_{10}\gamma_J^2(r_B) = -\frac{\log_{10}\mathbf{e}^2}{\hbar\omega}\left[\frac{2Z_D e^2}{r_B} - (Q_\alpha - E_J)\right] + \log_{10}\frac{\hbar^2 \mathcal{A}_J^2}{2\mathbf{e}\mu r_B} \ , \tag{3.63}$$

where $\mathbf{e} \approx 2.71828$, $e^2 = 1.44$ MeV $\cdot$ fm, Z_D denotes the charge number of the daughter nucleus and $\mathcal{A}_J$ is the amplitude of the Gaussian-like wave function peaked on the nuclear surface. This law together with (3.62) has the following consequences:

1) The Viola-Seaborg rule for the total half-life [60]

$$log_{10}T = \frac{aZ_D + b}{\sqrt{Q_\alpha}} + cZ_D + d \ ; \tag{3.64}$$

2) The logarithm of the HF becomes proportional to the excitation energy of the daughter nucleus [57]

$$\begin{aligned} log_{10}HF_J &= \frac{log_{10}\mathbf{e}^2}{\hbar\omega}E_J + log_{10}\frac{\mathcal{A}_0^2}{\mathcal{A}_J^2} \\ &\equiv e_J E_J + f_J \ ; \end{aligned} \tag{3.65}$$

3) By using Eq. (3.58) one obtains a similar rule for intensities

$$\Upsilon_J = g_J E_J + h_J \ . \tag{3.66}$$

4 Transitions from even-even emitters

We considered only even-even emitters with known α-decay half-lives, fulfilling the vibrational/rotational condition within an error of 10% for the first four excited states

$$\frac{J+2}{J}(1-0.1) \leq \frac{E_{J+2}}{E_J} \leq \frac{(J+2)(J+3)}{J(J+1)}(1+0.1),\ J=2,4,6,8. \qquad (4.1)$$

In the numerical analysis we chose the model parameters according to the following procedure:

- the CSM deformation parameter d defined by Eq. (3.1) and
- the CSM Hamiltonian parameter A_1 defined by Eq. (3.7)

were determined by fitting the experimental energy levels E_J of the first four excited states according to Eq. (3.7) for each nuclide where the data was available. The relative errors of the 2^+ state and the resulting parameters are given in Table 2. In this Table the used notations are given below

n:	nuclide label
D(J):	even Z - even N daughter nuclide
d:	CSM deformation parameter defined by Eq. (3.1), fitted for each case
A_1 (keV):	CSM Hamiltonian parameter defined by Eq. (3.7) (keV), fitted for each case
C:	α-daughter coupling strength defined by Eq. (3.41), reproducing the intensity Υ_2
Q (MeV) :	Q-Value of the decay process
$log_{10}T_\alpha$ (s) :	experimental and theoretical logarithm of total half-life
Υ_{J^+}:	Experimental and theoretical decay intensity to the state of angular momentum J

In Fig. 6 we plotted the CSM deformation parameter d versus the standard quadrupole deformation parameter β_2.

In Fig. 7 the ratio E_4/E_2 is plotted versus the CSM deformation parameter and shows a consensus with the prediction of Eq. (3.9), as is the situation for ratios of higher states.

The effective charge q_{eff} defined by Eq. (3.11) was extracted from the $B(E2 : 2 \rightarrow 0)$ value (3.10) for each nuclide. The dependence between the effective charge and the CSM deformation parameter is given in Fig. 9. The connection between the excitation energy E_2 divided by the Hamiltonian parameter A_1 and the B(E2)-value divided by the effective charge, predicted by Eq. (3.14), is plotted in Fig. 10.

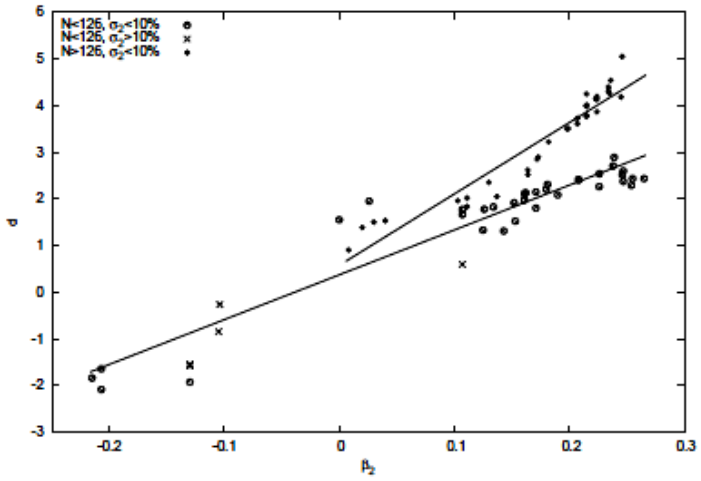

Figure 6: The CSM deformation parameter versus quadrupole deformation parameter.

Table 2: Parameters and fine structure decay data for even-even daughter nuclei.

n	$D(J)$	d	A_1 (keV)	C	Q (MeV)	$\log_{10} T_\alpha^{exp}$ (s)	$\log_{10} T_\alpha^{pred}$ (s)	$\Upsilon_{2^+}^{exp}$	$\Upsilon_{2^+}^{pred}$	$I_{4^+}^{exp}$	$\Upsilon_{4^+}^{pred}$	$\Upsilon_{6^+}^{exp}$	$\Upsilon_{6^+}^{pred}$
1	$^{154}_{68}Er_{86}$	1.311	608.286	0.507	4.172	6.7	7.157	-	3.833	-	-	-	-
2	$^{156}_{70}Yb_{86}$	1.329	595.022	0.503	4.902	3.1	3.545	3.0	3.009	-	-	-	-
3	$^{158}_{70}Yb_{88}$	1.976	712.321	0.350	4.417	5.8	6.183	2.3	2.382	-	-	-	-
4	$^{158}_{72}Hf_{86}$	1.666	665.332	0.423	5.674	0.5	0.816	-	2.171	-	-	-	-
5	$^{160}_{72}Hf_{88}$	1.914	720.777	0.364	5.279	2.2	2.490	2.0	2.027	-	-	-	-
6	$^{162}_{72}Hf_{90}$	2.200	781.036	0.297	4.856	4.7	5.116	-	1.482	-	-	-	-
7	$^{164}_{72}Hf_{92}$	2.404	771.313	0.248	4.506	6.3	6.762	1.3	1.352	-	-	-	-
8	$^{164}_{74}W_{90}$	2.108	802.813	0.318	5.818	0.7	0.949	1.2	1.541	-	-	-	-
9	$^{166}_{74}W_{92}$	2.310	808.548	0.271	5.539	1.9	2.132	1.2	1.275	-	-	-	-
10	$^{168}_{74}W_{94}$	2.411	743.663	0.247	5.227	3.3	3.546	1.0	1.132	-	-	-	-
11	$^{170}_{74}W_{96}$	2.536	689.780	0.217	4.872	5.3	5.598	1.0	0.922	-	-	-	-
12	$^{164}_{76}Os_{88}$	0.596	581.877	0.677	6.999	-2.7	-2.702	-	3.471	-	-	-	-
13	$^{166}_{76}Os_{90}$	1.827	759.231	0.385	6.708	-1.9	-1.750	-	2.626	-	-	-	-
14	$^{168}_{76}Os_{92}$	2.132	856.069	0.313	6.464	-1.0	-0.774	1.4	1.392	-	-	-	-
15	$^{170}_{76}Os_{94}$	2.144	757.750	0.310	6.184	0.1	0.267	2.0	1.277	-	-	-	-
16	$^{172}_{76}Os_{86}$	2.085	572.757	0.324	5.887	1.2	1.375	2.6	1.154	-	-	-	-
17	$^{174}_{76}Os_{98}$	2.262	492.509	0.282	5.573	2.6	2.800	1.3	0.895	-	-	-	-
18	$^{176}_{76}Os_{100}$	2.517	577.809	0.221	5.240	4.3	4.481	0.8	0.791	-	-	-	-
19	$^{178}_{76}Os_{102}$	2.598	629.969	0.202	4.952	5.5	5.803	0.7	0.898	-	-	-	-
20	$^{180}_{76}Os_{104}$	2.706	713.724	0.177	4.602	8.0	8.335	0.9	0.818	-	-	-	-
21	$^{182}_{76}Os_{106}$	2.892	820.202	0.133	4.320	9.7	10.164	0.9	0.810	-	-	-	-
22	$^{168}_{78}Pt_{90}$	-0.549	556.997	0.948	7.525	-3.6	-3.596	1.9	3.890	-	-	-	-
23	$^{170}_{78}Pt_{92}$	1.773	822.277	0.398	7.233	-2.7	-2.622	-	2.898	-	-	-	-
24	$^{172}_{78}Pt_{94}$	1.778	753.771	0.397	6.908	-1.6	-1.565	1.7	2.745	-	-	-	-
25	$^{174}_{78}Pt_{96}$	1.524	508.800	0.457	6.578	-0.6	-0.330	1.4	1.610	-	-	-	-
26	$^{176}_{78}Pt_{98}$	1.803	408.928	0.391	6.258	0.7	0.919	3.3	1.195	-	-	-	-

n	$D(J)$	d	A_1 (keV)	C	Q (MeV)	$\log_{10} T_\alpha^{exp}$ (s)	$\log_{10} T_\alpha^{pred}$ (s)	Υ_{2+}^{exp}	Υ_{2+}^{pred}	I_{4+}^{exp}	Υ_{4+}^{pred}	Υ_{6+}^{exp}	Υ_{6+}^{pred}
27	$^{178}_{78}Pt_{100}$	2.290	502.074	0.275	5.997	1.9	1.986	2.2	0.816	-	-	-	-
28	$^{180}_{78}Pt_{102}$	2.435	556.229	0.241	5.662	3.5	3.672	2.4	0.701	-	-	-	-
29	$^{182}_{78}Pt_{104}$	2.433	567.247	0.241	5.205	5.7	6.002	0.9	0.816	-	-	-	-
30	$^{184}_{78}Pt_{106}$	2.374	556.438	0.255	4.705	8.9	9.155	1.1	0.913	-	-	-	-
31	$^{176}_{80}Hg_{96}$	-0.847	607.326	1.019	7.415	-2.4	-2.218	2.0	2.069	-	-	-	-
32	$^{182}_{80}Hg_{102}$	-0.798	566.771	1.007	6.470	1.1	1.268	2.8	1.439	-	-	-	-
33	$^{184}_{80}Hg_{104}$	-1.542	582.367	1.183	6.109	2.4	2.276	3.0	1.744	-	-	-	-
34	$^{186}_{80}Hg_{106}$	-1.578	623.792	1.192	5.698	4.3	4.524	3.1	2.111	-	-	-	-
35	$^{188}_{80}Hg_{108}$	-1.926	831.157	1.274	5.221	4.6	5.442	2.4	2.668	-	-	-	-
36	$^{190}_{80}Hg_{110}$	-0.875	570.462	1.025	4.738	10.0	10.493	2.8	2.979	-	-	-	-
37	$^{206}_{82}Pb_{124}$	0.296	549.153	0.748	5.407	7.1	8.524	5.0	3.882	-	-	-	-
38	$^{208}_{82}Pb_{126}$	0.576	506.032	0.798	8.954	-6.5	-6.628	-	2.042	-	5.542	-	11.190
39	$^{214}_{82}Pb_{132}$	0.714	482.106	0.771	6.115	2.3	2.651	5.0	4.763	-	6.705	-	15.190
40	$^{192}_{84}Po_{108}$	-2.086	580.790	1.312	7.617	-2.4	-2.524	-	1.194	-	-	-	-
41	$^{194}_{84}Po_{110}$	1.948	576.364	0.356	7.349	-1.2	-1.350	3.2	1.477	-	-	-	-
42	$^{196}_{84}Po_{112}$	1.551	537.982	0.450	7.043	-0.009	0.209	4.2	2.606	-	-	-	-
43	$^{198}_{84}Po_{114}$	0.373	550.372	0.730	6.774	1.1	1.523	3.7	2.417	-	-	-	-
44	$^{200}_{84}Po_{116}$	0.459	552.127	0.709	6.545	2.0	2.483	-	2.838	-	-	-	-
45	$^{202}_{84}Po_{118}$	0.459	552.127	0.709	6.384	2.7	3.228	-	2.997	-	-	-	-
46	$^{208}_{84}Po_{124}$	0.200	548.082	0.771	6.385	3.2	3.760	3.3	2.843	-	-	-	-
47	$^{198}_{86}Rn_{112}$	-1.837	579.035	1.253	8.019	-1.8	-1.713	-	1.034	-	-	-	-
48	$^{200}_{86}Rn_{114}$	-1.641	593.863	1.207	7.636	-1.2	-0.655	-	1.089	-	-	-	-
49	$^{206}_{86}Rn_{120}$	-0.049	547.653	0.830	7.152	0.6	0.937	3.5	2.128	-	-	-	-
50	$^{216}_{86}Rn_{130}$	0.906	405.170	0.733	7.592	-1.8	-1.173	2.0	1.889	-	4.707	-	9.274
51	$^{218}_{86}Rn_{132}$	1.532	385.309	0.608	6.679	1.6	2.333	1.5	1.489	4.4	4.329	-	8.879
52	$^{220}_{86}Rn_{134}$	1.835	398.646	0.548	5.789	5.5	6.368	1.3	1.310	4.1	4.254	-	9.096
53	$^{222}_{86}Rn_{136}$	2.047	410.960	0.506	4.871	10.7	11.644	1.2	1.270	4.2	4.437	-	9.909
54	$^{208}_{88}Ra_{120}$	-0.265	549.718	1.634	7.952	-1.5	-1.423	1.6	2.967	-	-	-	-
55	$^{218}_{88}Ra_{130}$	1.388	405.293	0.637	8.127	-2.7	-1.962	1.6	1.421	-	3.979	-	8.323
56	$^{220}_{88}Ra_{132}$	1.959	344.753	0.523	7.298	0.04	0.896	0.6	0.690	-	2.891	-	6.793
57	$^{222}_{88}Ra_{134}$	2.353	376.272	0.445	6.451	3.3	4.153	0.5	0.472	2.6	2.606	-	6.744
58	$^{224}_{88}Ra_{136}$	2.616	402.858	0.392	5.520	7.8	8.660	0.4	0.444	2.5	2.677	6.5	6.767
59	$^{226}_{88}Ra_{138}$	2.851	418.088	0.346	4.770	12.4	13.242	0.5	0.442	2.8	2.737	7.0	7.232
60	$^{228}_{88}Ra_{140}$	3.327	501.339	0.251	4.083	17.6	18.449	0.6	0.572	3.1	3.205	-	8.033
61	$^{220}_{90}Th_{130}$	1.502	437.194	0.614	8.620	-3.1	-2.456	1.1	1.342	-	4.087	-	9.008
62	$^{222}_{90}Th_{132}$	2.018	391.376	0.511	7.715	-0.5	0.321	0.8	0.689	-	2.989	-	7.093
63	$^{224}_{90}Th_{134}$	2.519	416.728	0.412	6.804	2.8	3.571	0.4	0.404	2.1	2.498	-	7.858
64	$^{226}_{90}Th_{136}$	2.895	464.030	0.337	5.993	6.3	7.076	0.3	0.349	2.2	2.442	6.0	6.868
65	$^{228}_{90}Th_{138}$	3.221	492.731	0.272	5.414	9.3	10.093	0.3	0.340	2.4	2.500	6.1	5.556
66	$^{230}_{90}Th_{140}$	3.499	555.671	0.217	4.860	12.9	13.581	0.4	0.415	2.6	2.603	-	5.706
67	$^{232}_{90}Th_{142}$	3.608	555.049	0.195	4.573	14.9	15.540	0.5	0.418	2.7	2.858	5.7	5.076
68	$^{234}_{90}Th_{144}$	3.767	615.270	0.163	4.270	17.2	17.801	0.6	0.495	3.0	2.912	-	6.938
69	$^{226}_{92}U_{134}$	3.205	480.365	0.275	7.175	2.0	2.534	-	0.216	-	2.058	-	5.403
70	$^{228}_{92}U_{136}$	3.495	533.395	0.217	6.716	3.9	4.528	0.3	0.320	-	2.317	-	4.723
71	$^{230}_{92}U_{138}$	3.508	543.762	0.215	6.310	5.7	6.321	0.3	0.301	2.2	2.351	-	5.311
72	$^{232}_{92}U_{140}$	3.727	576.660	0.171	5.867	7.0	8.512	0.3	0.354	2.5	2.696	4.6	4.041
73	$^{234}_{92}U_{142}$	3.787	547.554	0.159	5.593	9.5	9.991	0.4	0.368	2.9	2.515	4.4	6.092
74	$^{236}_{92}U_{144}$	3.988	640.669	0.119	5.256	11.3	11.864	0.4	0.472	2.9	2.985	4.8	4.410
75	$^{238}_{92}U_{146}$	3.990	636.205	0.119	4.984	13.1	13.622	0.5	0.490	3.4	2.930	4.9	5.355
76	$^{240}_{92}U_{148}$	4.132	698.539	0.091	4.665	15.4	15.912	0.6	0.640	-	2.776	-	3.648
77	$^{234}_{94}Pu_{140}$	3.878	620.106	0.141	6.620	5.3	5.810	0.4	0.381	-	2.827	-	3.618
78	$^{236}_{94}Pu_{142}$	4.012	640.608	0.115	6.398	6.4	6.813	0.4	0.465	3.1	2.424	3.7	3.319
79	$^{238}_{94}Pu_{144}$	4.248	718.871	0.068	6.216	7.2	7.520	0.5	0.682	3.3	3.319	4.2	5.394
80	$^{240}_{94}Pu_{146}$	4.138	659.043	0.090	5.902	8.8	9.178	0.5	0.554	3.6	2.623	4.3	3.315

n	$D\,(J)$	d	A_1 (keV)	C	Q (MeV)	$\log_{10} T_\alpha^{exp}$ (s)	$\log_{10} T_\alpha^{pred}$ (s)	$\Upsilon_{2^+}^{exp}$	$\Upsilon_{2^+}^{pred}$	$I_{4^+}^{exp}$	$\Upsilon_{4^+}^{pred}$	$\Upsilon_{6^+}^{exp}$	$\Upsilon_{6^+}^{pred}$
81	$^{242}_{94}Pu_{148}$	4.196	706.800	0.078	5.475	11.2	11.602	0.7	0.661	-	2.629	-	2.976
82	$^{244}_{94}Pu_{150}$	3.864	614.529	0.144	5.162	13.1	13.634	0.7	0.425	3.0	2.631	3.9	4.875
83	$^{246}_{96}Cm_{140}$	3.862	616.268	0.144	7.719	1.8	2.257	0.3	0.345	-	2.446	-	6.253
84	$^{248}_{96}Cm_{142}$	3.862	616.268	0.144	7.516	1.9	2.705	0.6	0.265	-	2.188	-	3.749
85	$^{250}_{96}Cm_{144}$	4.000	651.917	0.117	7.329	3.2	3.608	0.5	0.375	-	2.672	-	4.471
86	$^{252}_{96}Cm_{146}$	4.000	651.917	0.117	6.862	5.1	5.510	0.6	0.401	2.7	2.620	3.7	4.483
87	$^{254}_{96}Cm_{148}$	4.316	726.110	0.054	6.361	7.5	7.787	0.6	0.841	2.3	2.458	-	1.998
88	$^{256}_{96}Cm_{150}$	4.397	752.888	0.047	6.128	8.6	8.905	0.7	1.087	2.5	5.424	4.1	3.361
89	$^{258}_{96}Cm_{152}$	4.260	710.991	0.038	6.217	7.9	8.279	0.7	0.662	2.5	4.283	4.6	2.931
90	$^{260}_{96}Cm_{154}$	4.015	656.032	0.114	5.926	9.2	9.705	0.7	0.399	-	2.758	-	4.202
91	$^{242}_{98}Cf_{144}$	4.000	651.917	0.117	8.374	0.1	0.385	0.6	0.340	-	2.490	-	3.385
92	$^{244}_{98}Cf_{146}$	4.153	694.452	0.087	8.002	1.6	1.848	0.6	0.492	-	2.846	-	5.431
93	$^{246}_{98}Cf_{148}$	4.153	694.452	0.087	7.556	3.3	3.600	0.7	0.542	-	2.710	-	3.571
94	$^{248}_{98}Cf_{150}$	4.168	698.875	0.084	7.153	5.0	5.306	0.7	0.580	1.9	2.571	3.6	2.913
95	$^{250}_{98}Cf_{152}$	4.184	678.191	0.080	7.307	4.1	4.354	0.8	0.443	2.0	2.519	4.1	2.857
96	$^{252}_{98}Cf_{154}$	4.183	703.329	0.081	7.027	5.1	5.395	0.8	0.535	-	2.609	-	3.202
97	$^{248}_{100}Fm_{148}$	4.168	698.875	0.084	8.549	0.6	0.881	0.5	0.538	-	2.511	-	2.813
98	$^{250}_{100}Fm_{150}$	4.168	698.875	0.084	8.226	1.8	2.046	0.8	0.563	-	2.702	-	3.331
99	$^{252}_{100}Fm_{152}$	4.321	744.797	0.053	8.581	0.5	0.653	0.8	0.496	-	2.902	-	3.767
100	$^{252}_{102}No_{150}$	4.537	874.740	0.010	8.930	0.3	-0.981	-	2.317	-	1.068	-	-
101	$^{254}_{102}No_{152}$	5.051	1042.172	-0.092	9.250	-1.0	-0.946	-	0.938	-	2.857	-	3.389
102	$^{256}_{104}Rf_{152}$	4.351	754.351	0.047	9.923	-2.1	-2.052	0.7	0.823	-	2.933	-	2.456
103	$^{262}_{104}Rf_{158}$	4.076	672.800	0.102	8.762	2.1	2.423	-	0.869	-	1.725	-	1.515
104	$^{260}_{106}Sg_{154}$	4.229	716.874	0.071	10.591	-2.8	-2.733	-	0.607	-	3.218	-	3.716
105	$^{262}_{106}Sg_{156}$	4.076	672.800	0.102	10.335	-2.7	-2.501	-	0.351	-	2.295	-	3.776
106	$^{266}_{106}Sg_{160}$	4.092	677.069	0.099	9.300	0.6	0.820	-	0.460	-	2.505	-	3.480
107	$^{266}_{108}Hs_{158}$	4.092	677.069	0.099	11.200	-4.0	-3.929	-	0.357	-	2.471	-	3.888
108	$^{280}_{110}Ds_{170}$	2.227	383.511	0.470	9.349	1.0	2.043	-	0.281	-	2.050	-	4.994
109	$^{284}_{112}Cn_{172}$	1.936	379.034	0.528	10.090	-0.1	0.877	-	0.514	-	2.486	-	5.821
110	$^{288}_{114}Fl_{174}$	1.386	401.032	0.637	10.800	-1.8	-0.767	-	0.982	-	3.117	-	6.410
111	$^{290}_{116}Lv_{174}$	1.677	384.449	0.579	11.810	-2.8	-1.924	-	0.739	-	2.872	-	6.568

The monopole potential strength v_a defined by Eq. (3.34) was fixed by the total α-decay half-life. The repulsive strength c defined by Eq. (3.34) has the value $c = 50$ MeV, suggested by Ref. [44]. The α-daughter coupling strength C defined by Eq. (3.41) was obtained from the reproduced values of the α-decay intensity Υ_2 (3.54). We compared our results with the experimental data available and made predictions for the nuclei where these observables have not been measured to this date, separately for two regions, namely $N < 126$ and $N > 126$. Thus, we computed

- the energies of the daughter nucleus E_J by using

a) the linear dependence between d and β_2 (given by Ref. [77]) predicted by Eq. (3.2) and evidenced in Fig. 6, and

b) the quadratic dependence between the Hamiltonian strength A_1 of Eq. (3.7) and the CSM deformation parameter d evidenced in Fig. 8;

- the $B(E2)$ values by using the linear relation (3.11) between the effective charge q_{eff} and d evidenced in Fig. 9;

- half-lives given in Fig. 14, by using the quadratic dependence between v_a and the square of the reduced width γ_0^2 in Fig. 13;

- intensities Υ_J (3.54) given in Fig. 16, by using the linear dependence (3.41) between the α-daughter strength C and d shown in Fig. 15, panel (a). The logarithms of hindrance factors, given by Eq. (3.65), have a similar behavior as the intensities and therefore we will not plot these quantities.

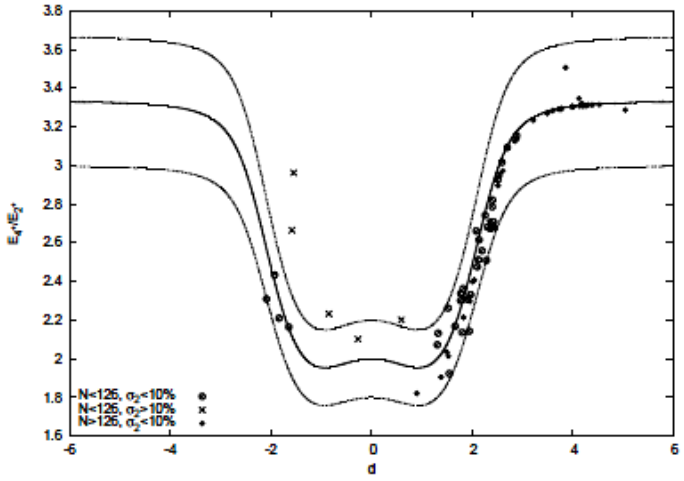

Figure 7: Experimental energy ratio versus the CSM deformation parameter for J=2.

The α-decay spectrum is a very sensitive tool for the investigation of nuclear structure. Thus, the intriguing maximum of the HF, or equivalently, the maximum of the intensity Υ_J for the 4^+ state in the Pu region evidenced in Ref. [43] was recently related to the two-neutron separation energy, in connection to a deformed subshell corresponding to N=142 [78]. This effect can be seen where we plotted the experimental values of Υ_4 as a function of the Casten parameter $P = N_p N_n/(N_p + N_n)$.

In Fig. 15, panel (a), it can be observed that in the $N < 126$ region, for $C < 0.1$, the nuclei follow the general rule given by (3.41), but with a smaller slope.

For nuclei obeying the rule (3.41) with a larger slope, the value of C reproducing Υ_2 always corresponds to wave functions in antiphase. In panel (b) we plotted the same dependence for $^{194}_{86}\mathrm{Po}_{108}$. In this case, solutions in antiphase do not exist for the given excitation energy, and Υ_2 is reproduced by a value of C corresponding to a solution with the wave functions in phase. This is the situation for all nuclei having $C < 0.1$, where the dependence $C(d)$ has a smaller slope.

Notice that for nuclei where there is no experimental data concerning alpha-branching ratios we assumed that the branch to the ground state is unity.

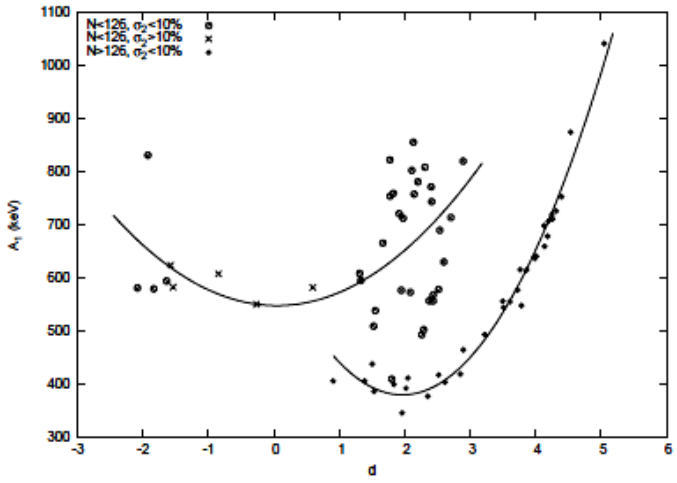

Figure 8: Hamiltonian strength parameter versus the CSM deformation parameter.

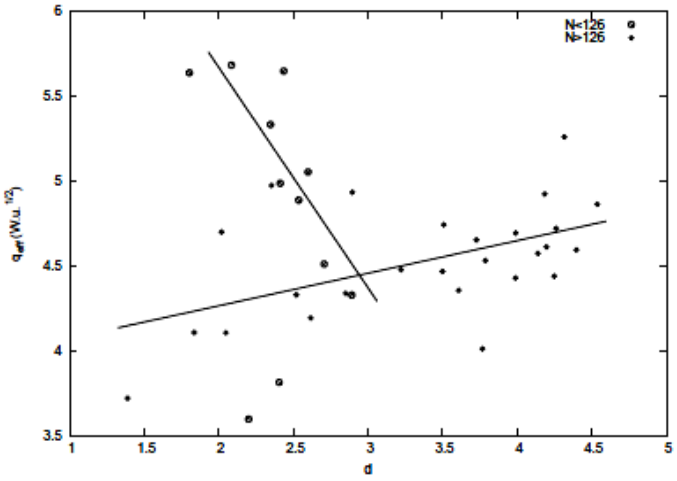

Figure 9: Effective charge versus the CSM deformation parameter.

We clearly evidenced several α-clustering properties, i.e.:

- a large correlation between the monopole potential strength v_a (measuring the departure from the "pure" α-core picture with $v_a = 1$) and preformation probability γ_0^2 in Fig. 13;

- a large correlation between the α-daughter quadrupole coupling strength C and preformation probability γ_0^2 in Fig. 15, panel (b).

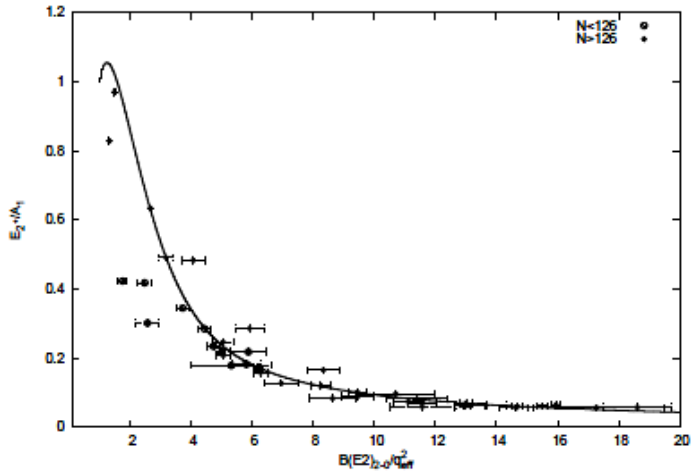

Figure 10: $E_{2^+}/A_1(d)$ versus $B(E2;2 \to 0)/q^2_{eff}(d)$.

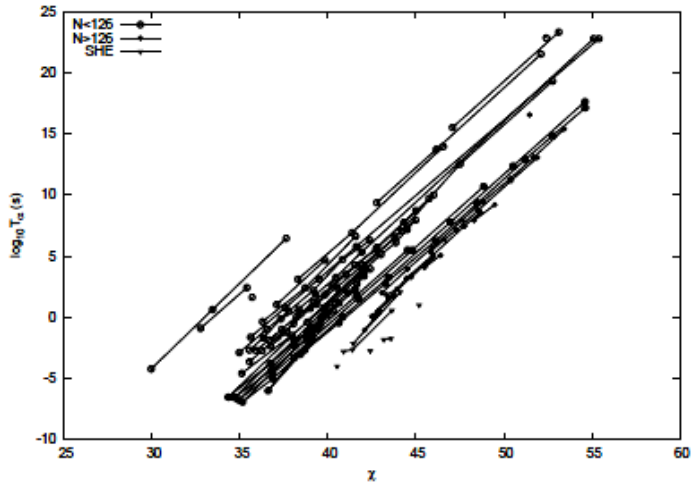

Figure 11: Logarithm of the half-life versus the Coulomb parameter for J=0.

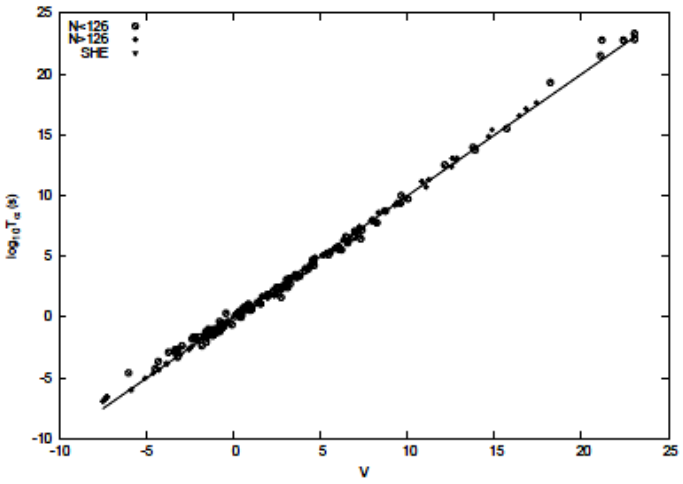

Figure 12: Logarithm of the half-life versus the Viola-Seaborg parameter.

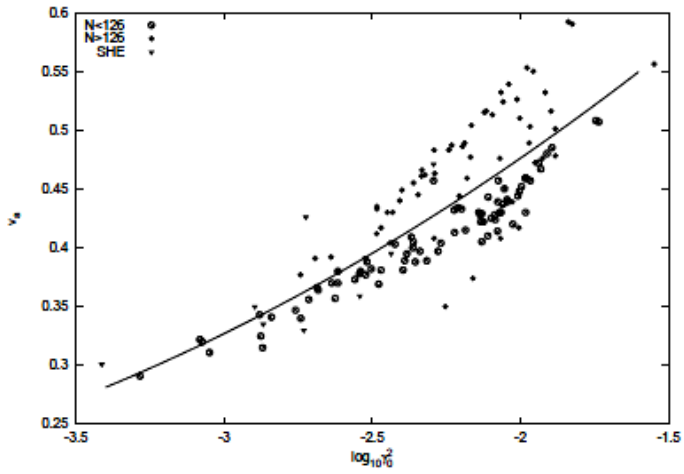

Figure 13: Potential parameter v_a versus the logarithm of the squared reduced width.

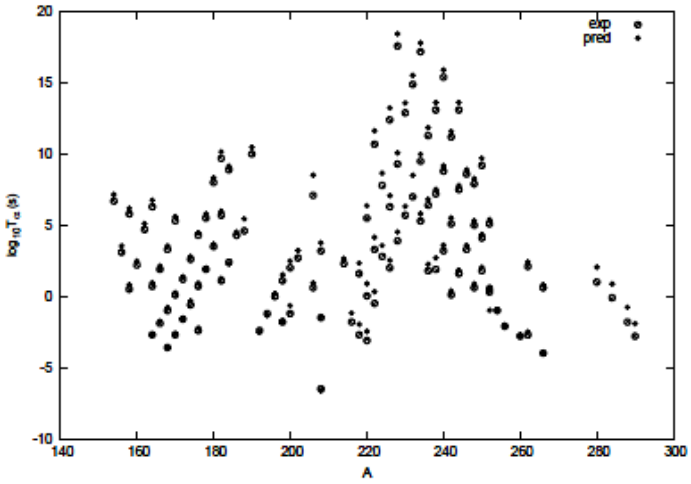

Figure 14: Logarithm of the half-life versus mass number.

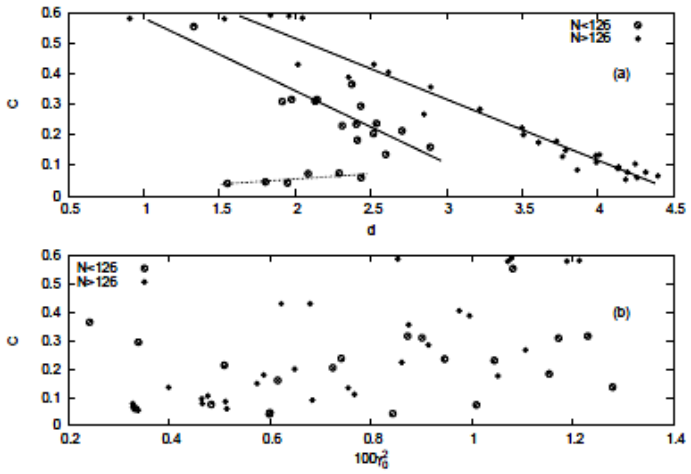

Figure 15: Panel (a) shows the α-core coupling strength versus the CSM deformation parameter. Panel (b) shows the α-core coupling strength versus the square of the reduced width multiplied by 100.

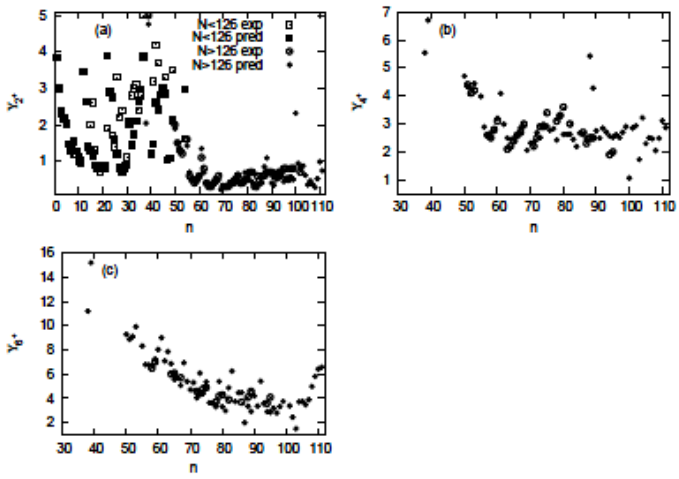

Figure 16: Panel (a) shows the intensity Υ_2 versus the number labeling each nucleus. The same is true for panel (b) for $J = 4$ and panel (c) for $J = 6$.

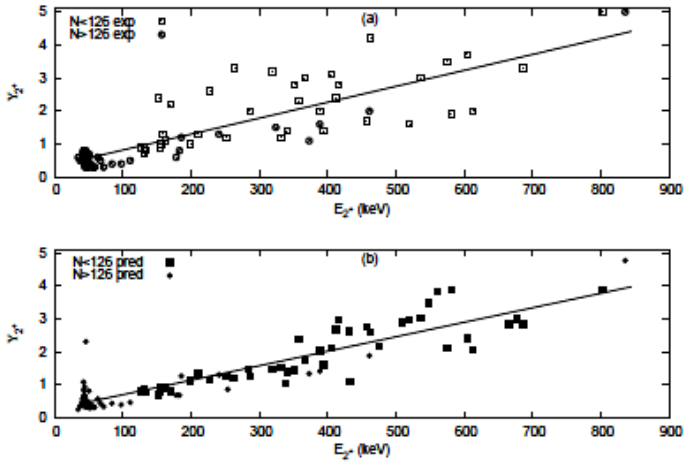

Figure 17: The intensity Υ_2 versus the excitation energy E_2 of the daughter nucleus.

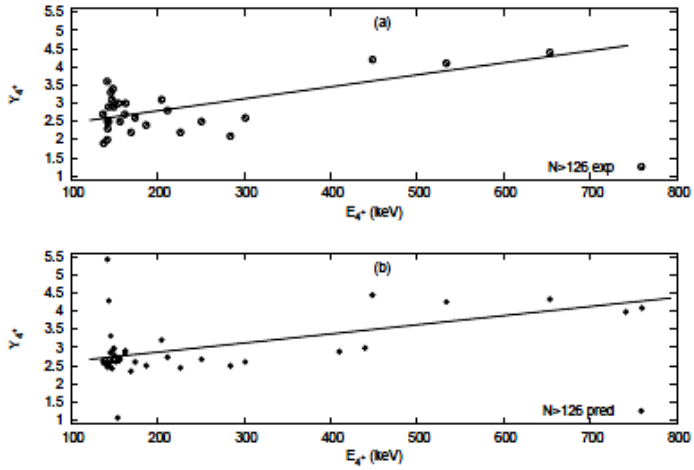

Figure 18: Same as in Fig. 18 for J=4.

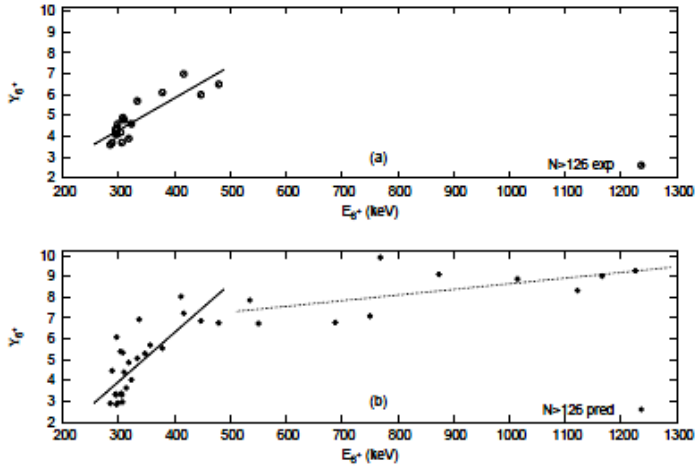

Figure 19: Same as in Fig. 17 for J=6.

5 Favored transitions from odd-mass emitters

We have studied favored transitions in 26 odd-mass α-emitters where the rotational band in which the parent decays is built atop a single particle orbital of angular momentum projection $\Omega \neq \frac{1}{2}$. Additionally, this band must be described in the formalism of an odd nucleon coupled to good angular momentum with a CSM core.

The deformation parameter d was obtained by fitting available energy levels relative to the bandhead. A number of about 4 levels is required for the determination of a reliable deformation. As can be seen from Fig. 5, there exists a deformation range where a large shift of the parameter's value has little impact on the energy levels. Because of this, when fewer energy levels are available, the fit becomes unreliable. In these circumstances we have determined the deformation parameter by studying the systematics of energy levels and deformations for the neighboring nuclei with good experimental data. A quadratic trend is observed in the dependence of the Hamiltonian stregth parameter A_1 on the deformation, as evidenced in Fig. 20, where we assign the nuclei with separate symbols for each value of Ω. The fitting formula agrees qualitatively with the similar treatment made for the ground bands of even-even nuclei in Ref. [58]. The agreement between the ratio of experimental energy levels assigned to the deformation parameter d and the theoretical ratio $\frac{E_{I+1}}{E_I}$ is shown in Fig. 21, with separate panels for different values of Ω.

On the topic of electromagnetic transitions, one notices a surprising lack of measured $B(E2)$ values for odd-mass α-emitters. Only one such value can be found in the database, for the transition $\frac{9}{2}^+ \to \frac{5}{2}^+$ in the ground band of Th_{229}. It is given by

$$B\left(E2; \frac{9}{2}^+ \to \frac{5}{2}^+\right) = 170 \ \textit{30} \text{ W.u.}. \tag{5.1}$$

Using the systematics for the collective effective charge q_0^c as function of d established in Ref. [58] our model predicts a value

$$B\left(E2; \frac{9}{2}^+ \to \frac{5}{2}^+\right) = 117.8 \text{ W.u.}. \tag{5.2}$$

The difference up to the experimental value can be obtained by tweaking the value of the single particle effective charge q_0^{sp}, which in this case must be equal to $q_0^{sp} = 7.004$ $(\text{W.u.})^{\frac{1}{2}}$. Due to the lack of experimental data, a systematics of single particle effective charges cannot currently be made, but we present predictions for $B\left(E2; \Omega + 2 \to \Omega\right)$ values based on the systematics of the collective effective charge from Ref. [58].

To study α-transitions, we make use of the so-called decay intensities

$$\Upsilon_{Il} = \log_{10} \frac{\Gamma_{\Omega 0}}{\Gamma_{Il}}, \tag{5.3}$$

Table 3: Parameters and fine structure decay data for odd-mass daughter nuclei.

n	$D\,(I)$	d	A_1	C	$Q_{g.s.\to\Omega}$ (MeV)	$\log_{10} T_\alpha^{exp}$ (s)	$\log_{10} T_\alpha^{pred}$ (s)	Υ_1^{exp}	Υ_1^{pred}	Υ_2^{exp}	Υ_2^{pred}	Υ_3^{exp}	Υ_3^{pred}
1	$^{225}_{88}Ra_{137}$	3.804	475.876	0.107	4.931	11.4	10.477	0.8	0.779	1.8	1.672	2.7	2.820
2	$^{223}_{89}Ac_{134}$	2.496	181.721	0.073	6.580	3.4	1.819	0.6	0.319	1.3	1.287	2.1	2.424
3	$^{225}_{89}Ac_{136}$	3.066	305.552	0.085	5.679	7.4	6.168	0.6	0.342	1.3	1.324	-	2.455
4	$^{229}_{90}Th_{139}$	3.716	458.930	0.133	4.909	12.7	11.677	0.8	0.809	1.7	1.720	3.3	2.795
5	$^{231}_{90}Th_{141}$	3.589	490.657	0.112	4.290	16.3	16.291	1.3	1.301	2.6	2.402	-	3.990
6	$^{231}_{91}Pa_{140}$	3.984	702.273	0.052	5.011	12.1	11.392	1.2	1.231	2.1	2.124	-	3.815
7	$^{233}_{91}Pa_{142}$	3.700	587.036	0.061	4.720	13.8	13.394	1.2	1.238	2.3	2.226	-	3.804
8	$^{237}_{92}U_{145}$	3.775	489.617	0.114	4.980	13.3	12.095	0.8	0.841	1.8	1.747	3.4	2.847
9	$^{235}_{93}Np_{142}$	3.824	463.486	0.107	5.874	8.6	7.206	0.8	0.777	1.6	1.589	-	2.552
10	$^{237}_{93}Np_{144}$	3.817	496.159	0.104	5.578	10.1	8.831	0.8	0.814	1.7	1.647	3.8	2.714
11	$^{239}_{93}Np_{146}$	3.738	472.328	0.083	5.364	11.4	10.046	0.9	0.898	1.8	1.736	4.0	2.932
12	$^{239}_{94}Pu_{145}$	3.704	478.740	0.115	5.883	9.0	7.583	0.8	0.783	1.7	1.599	3.4	2.656
13	$^{241}_{94}Pu_{147}$	3.502	434.114	0.069	5.447	11.4	9.997	1.3	1.267	2.5	2.114	4.3	3.736
14	$^{241}_{95}Am_{146}$	3.449	432.807	0.033	5.983	8.6	7.337	1.2	1.201	1.4	1.170	-	3.789
15	$^{243}_{95}Am_{148}$	3.465	409.433	0.061	5.623	10.6	9.447	0.8	0.811	1.5	1.639	-	2.799
16	$^{245}_{95}Am_{150}$	3.389	467.904	0.042	5.198	12.2	11.997	1.7	1.655	-	2.656	-	4.669
17	$^{243}_{96}Cm_{147}$	3.040	281.795	0.070	6.400	7.5	5.699	1.3	1.283	-	2.003	-	3.587
18	$^{245}_{96}Cm_{149}$	3.667	395.789	0.093	5.908	10.0	8.278	1.2	1.241	2.4	1.956	4.1	3.477
19	$^{249}_{96}Cm_{153}$	3.511	460.624	0.065	6.077	8.7	7.274	1.3	1.250	-	2.055	-	3.625
20	$^{241}_{97}Bk_{144}$	3.433	380.147	0.052	7.858	2.2	0.125	0.8	0.786	1.4	1.524	-	2.624
21	$^{247}_{97}Bk_{150}$	3.281	332.176	0.042	6.597	7.1	5.161	0.9	0.930	1.4	1.703	-	3.008
22	$^{249}_{97}Bk_{152}$	3.667	358.729	0.055	6.739	6.3	4.486	1.1	1.136	2.0	1.978	3.0	3.179
23	$^{251}_{97}Bk_{154}$	3.771	312.780	0.078	6.401	7.9	6.095	1.0	0.952	1.5	1.639	-	2.727
24	$^{247}_{98}Cf_{149}$	3.600	328.578	0.075	6.945	6.0	4.061	1.3	1.259	2.3	1.900	-	3.339
25	$^{251}_{98}Cf_{153}$	3.874	565.534	0.044	7.133	4.9	3.161	1.3	1.265	2.2	2.020	3.0	3.553
26	$^{253}_{98}Cf_{155}$	3.274	447.757	0.059	6.622	6.9	5.382	1.7	1.674	2.5	2.554	-	4.528

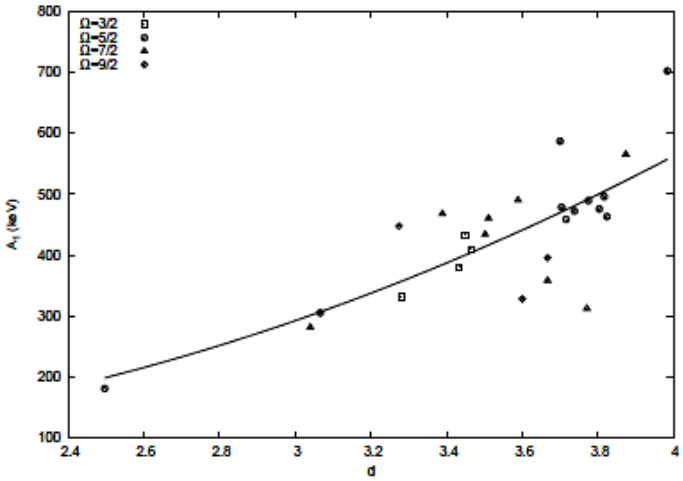

Figure 20: Hamiltonian strength parameter A_1 versus deformation d for rotational bands built atop different values of the odd nucleon angular momentum projection Ω.

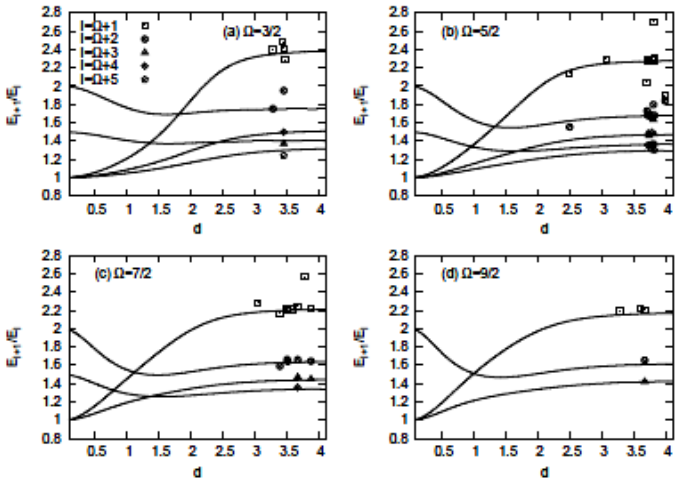

Figure 21: Experimental energy level ratios $\frac{E_{I+1}}{E_I}$ as a function of the deformation parameter d together with the theoretical curves, separately for each value of the single particle angular momentum projection Ω.

and we will employ the notation Υ_i, $i = 1, 2, 3$ to refer to decay intensities for the transitions to the first, second and third excited state respectively in any rotational band of bandhead angular momentum projection $\Omega \neq \frac{1}{2}$. Notice that, in principle, each intensity Υ_i is given by the sum

$$\Upsilon_i = \sum_l \Upsilon_{Il}, \tag{5.4}$$

where I is fixed by the angular momentum of the daughter nucleus in that particular state and l follows from the triangle rule for the coupling to total angular momentum I_P. However, it is sufficient to consider only one l-value for each state. This is due to the fact that the standard penetrability P_{Il} through the Coulomb barrier, defined by the usual factorization (2.7) decreases by one order of magnitude for each increasing value of l. Therefore, one would expect to be able to make a reasonable prediction of the fine structure of the α-emission spectrum using a basis of just four states, one state for the bandhead and an additional state for each excited energy level. In the cases where experimental data concerning the energy of the last state was not available, we used the CSM core + particle prediction provided by the fit of the lower energies.

It turns out however that the basis suggested above needs to be enlarged, due tot the fact that the parity of a resonance is fixed by whether the l-values involved are even or odd. Since the QQ interaction conserves parity, one must construct separate resonances of fixed even or odd parity. The even one follows the sequence of minimal l-values in each channel as $l = 0, 2, 2, 4$, while the odd one follows the sequence $l = 1, 1, 3, 3$. Thus, each basis of four states having

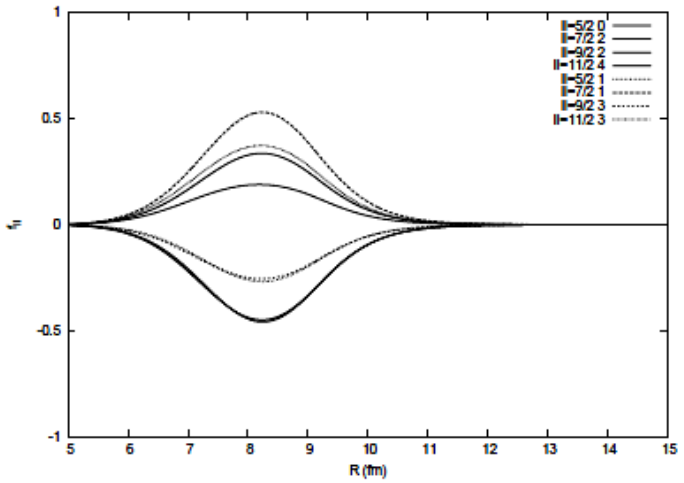

Figure 22: Solutions to the system (3.46) for the favored decay process $\mathrm{U}_{92}^{233} \rightarrow \mathrm{Th}_{92}^{229} + \alpha_2^4$. Solid lines represent radial functions of even orbital angular momentum l while dashed lines represent radial functions of odd l. The sets of functions fixed parity are obtained simultaneously for the same reaction energy and QQ coupling strength.

a given parity constructs a separate resonant solution of the system (3.46). It is important that both resonances are found at the same reaction energy Q_α and same QQ coupling stregth C. It is possible to achieve this for the potential of Eq. (3.34) by adjusting the depth v_0 so that both resonances generated at the same C match in terms of the reaction energy. Using this, one can then tweak the effective coupling strength C of Eq. (3.41) to simultaneously generate different sets of even and odd resonances for each α-decay process of energy Q_α, in an attempt to fit experimental data. One will thus obtain a total of eight radial functions in the solution, four in each resonance, as can be seen in Fig. 22 for the decay process

$$\mathrm{U}_{92}^{233} \rightarrow \mathrm{Th}_{92}^{229} + \alpha_2^4. \tag{5.5}$$

We have observed that for 23 decay processes out of the total of 26 studied, C can be tweaked in order to match the experimental value of Υ_1 for a decay width with $l = 0$ corresponding to the α-transition to the bandhead and the first decay width having $l = 2$ obtained in the even resonance corresponding to the α-transition to the first excited state. Simultaneously, the ratio between decay widths corresponding to the same $l = 0$ for the decay to the bandhead and the first value of $l = 3$ for the decay to the second excited state obtained in the odd resonance yielded a very good estimate of Υ_2, while the ratio between decay widths corresponding to $l = 0$ for the bandhead decay and $l = 4$ for the decay to the third excited state found in the even resonance have given a reasonable value for Υ_3. One of the exceptions is the decay to the daughter nucleus Am_{95}^{241},

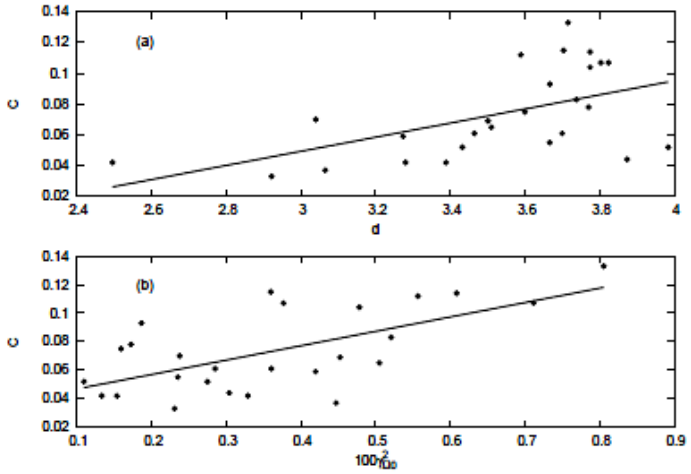

Figure 23: Panel (a) shows the effective α-nucleus coupling strength C versus deformation parameter d. Panel (b) presents the effective α-nucleus coupling strength C versus the reduced width $\gamma^2_{\Omega 0}$ for α-transitions to the bandhead.

where the available data concerning $\Upsilon_i, i = 1,2$ suggests a doublet structure in the emission spectrum that can be reproduced by employing the same $l = 0$ width for the bandhead transition and the two decay widths with $l = 2$ obtained in the even resonance. The other exception concerns the two Ac isotopes in our data set. In these cases, the decay width of angular momentum $l = 0$ and the first $l = 2$ obtained in the even resonance can be used to reproduce the value of Υ_2, situation in which the $l = 0$ width and the second width of angular momentum $l = 1$ in the odd resonance (which corresponds to the transition to the first excited state) will reproduce Υ_1 reasonably.

When plotted against the deformation parameter, the values of C obtained from the above fit follow the prediction of Eq. (3.41) by exhibiting a linear trend with respect to d, as seen in Fig. 23 panel (a). This coupling strength can be interpreted as a measure of α-clustering. To see this, we use the reduced width $\gamma^2_{\Omega 0}$ introduced in Eq. (2.7). It turns out that C shows a linear correlation with $\gamma^2_{\Omega 0}$ with a positive slope, as can be seen in Fig. 23 panel (b).

In Fig. 24 we present in separate panels the values of the intensities Υ_i, $i = 1,2,3$ obtained by the method presented above, versus the index number n found in the first column of Table 3. With open circles we show experimental data and with filled circles we give the values predicted by the coupled channels method with a particle + CSM core structure model. Dark triangles present the crudest barrier penetration calculation, where the intensities follow from the ratios of penetrabilities computed at the same values of l as in the coupled channels approach

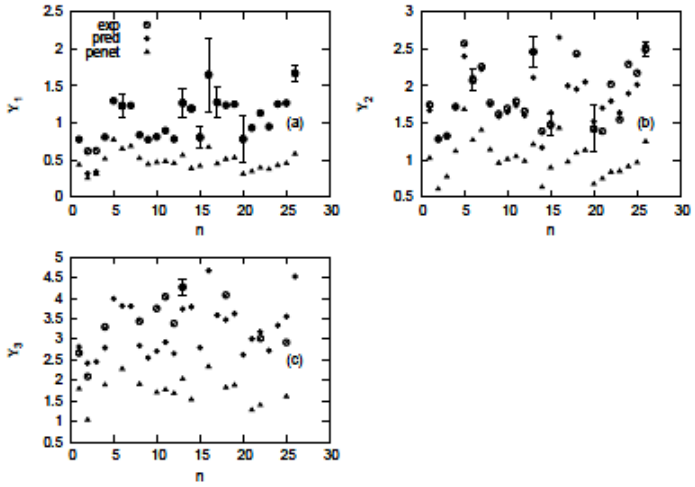

Figure 24: Intensities of the favored α-transitions Υ_i to the first three excited states in rotational bands as function of the index number n in the first column of Table 2. Open circles denote the experimental data, filled circles are the values predicted by the coupled channels method with a particle + CSM core structure model and dark triangles show the barrier penetration estimates.

$$\Upsilon_i = log_{10}\frac{P_{\Omega 0}}{P_{Il}}. \tag{5.6}$$

All emission data is presented in Table 3.

As we mentioned, the spectroscopic factor defined by Eq. (3.35) accounts for clustering effects. One can define partial spectroscopic factors for each channel and the logarithm of the hindrance factor as

$$\log_{10} HF_{Il} = \log \frac{S_{\Omega 0}}{S_{Il}} = \Upsilon_{Il}^{exp} - \Upsilon_{Il}^{theor}. \tag{5.7}$$

This quantity shows the importance of the extra-clustering in the decay process to excited states that is not considered within our model. In Fig. 25 we have plotted these logarithms versus the neutron number. It is clearly shown that coupling an α-particle to the daughter nucleus with the required strength needed to reproduce one intensity (usually Υ_1, with the exception of Ac isotopes where Υ_2 is reproduced) allows one to predict the values of the other intensities within a factor usually less than 3.

We note that the universal decay law treated in Refs. [3] and [79] is once again manifested in the dependence of the decay intensities on excitation energies. In Fig. 26 we have represented all of the Υ_i values as function of the corresponding excitation energy E_i relative to the bandhead for each collective structure analyzed in this paper. We observe a universal linear correlation with parameters

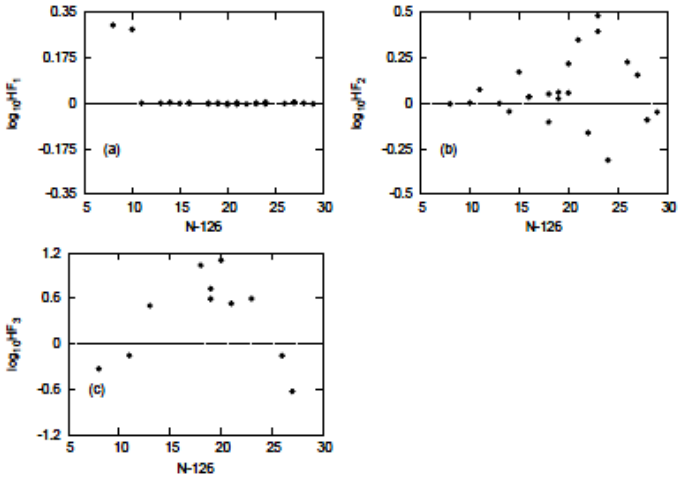

Figure 25: Logarithm of the hindrance factor HF_i versus neutron number $N-126$, separately for each excited state $i=1,2,3$.

$$\Upsilon_i = 0.017E_i + 0.169,\ \sigma = 0.316. \tag{5.8}$$

As a final remark, the logarithm of the spectroscopic factor of Eq. (3.35) can be represented as a function of neutron number, like in Fig. 27. This quantity shows a decreasing trend with the neutron number, meaning that the unquenched potential predicts shorter half-lives for heavier nuclei than what is observed experimentally.

6 Conclusions

We analyzed the available experimental α-decay widths to excited states for even-even and odd-mass emitters. We have shown that α-intensities to excited states depend linearly upon the excitation energy of the daughter nucleus in all known α-emission processes. We generalized the well known Viola-Seaborg law for α-transitions between ground states to the case of transitions to excited states, allowing for reliable predictions concerning the half-lives of α-transitions to any excited state.

We analyzed α-emitters with known decay widths between ground states by using the CSM formalism. Thus, we described in a unified way electromagnetic and α-transitions in vibrational, transitional and well deformed nuclei. We shown that the simplest harmonic CSM Hamiltonian is able to describe all available energy levels and electromagnetic transitions in terms of the CSM deformation parameter d, proportional to the standard quadrupole parameter β_2.

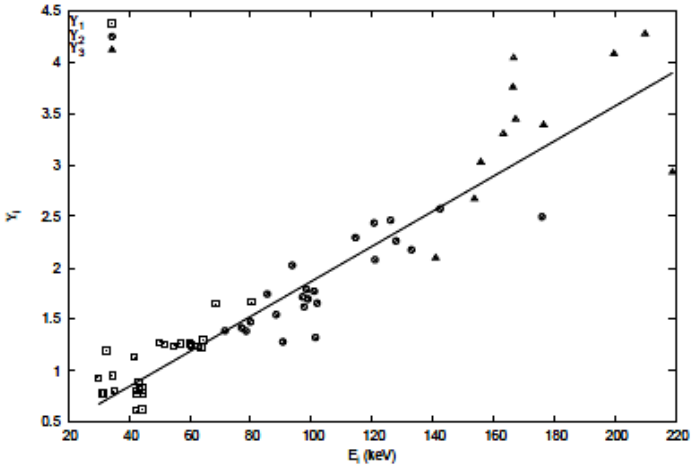

Figure 26: Υ_i values versus excitation energy E_i relative to the bandhead in each case.

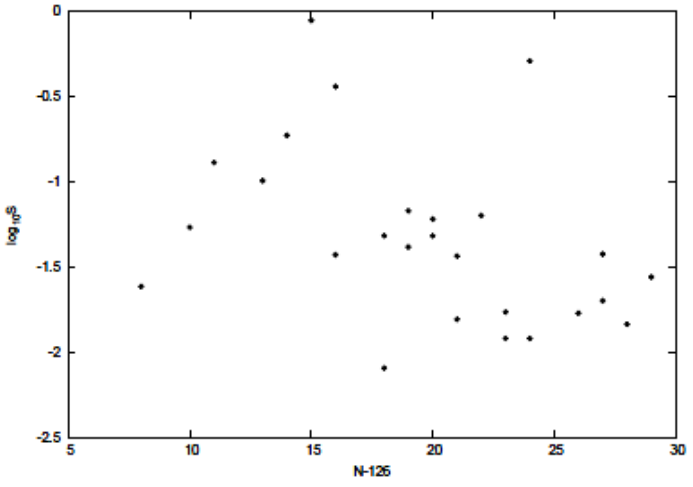

Figure 27: Logarithm of the spectroscopic factor S versus neutron number $N - 126$.

We used the same value of the CSM deformation parameter to study the α-decay fine structure in daughter nuclei within the coupled channels formalism. The attractive part of the monopole interaction was treated using the double folding procedure with a M3Y interaction, while a quadrupole-quadrupole ansatz was considered for the α-core interaction. The Pauli principle was simulated by a repulsive potential depending on one independent parameter. The first narrow resonant state in the resulting pocket-like potential was identified with an α-decaying state. Its eigenvalue was fixed to the experimental Q-value by using the depth of the monopole repulsive potential.

We reproduced the total half-life by using the parameter v_a multiplying the attractive monopole potential, and it turns out that this parameter is proportional to the α-particle formation probability. The intensity of α-transitions to 2^+ states was reproduced by using the quadrupole strength parameter C depending linearly on the deformation parameter, as predicted by the CSM. By using these values we were able to reproduce experimental intensities to 4^+ and 6^+ states with reasonable accuracy and we made theoretical predictions for other α-emitters.

We analyzed the available experimental data for favored α-transitions to rotational bands built upon a single particle angular momentum projection $\Omega \neq \frac{1}{2}$. The nuclear structure was modeled as an odd-nucleon coupled to a coherent state even-even core, the energy levels of each band being fitted through the use of a deformation parameter d and Hamiltonian strength parameter A_1 that is related to the deformation through a quadratic dependence. $B(E2)$ values can be predicted using the systematics of the collective effective charge as function of deformation established in Ref. [58]. In the absence of experimental data that allows the study of the single particle effective charge contribution, it is expected that these predicted values are smaller than what will be observed in reality.

The fine structure of the α-emission spectrum was studied using the coupled channels method, through a QQ interaction tweaked by a coupling strength that behaves linearly with respect to the deformation parameter and reduced width for the g.s.$\rightarrow \Omega$ transition. The predicted values of the intensities are in reasonable agreement with experimental data, usually within a factor less than 3.

References

[1] G. Gamow, Z. Phys. **51**, 204 (1928).

[2] E.U. Condon and R.W. Gurney, Nature **122**, 439 (1928).

[3] D. S. Delion, Phys. Rev. **C** 80, 024310 (2009).

[4] V.Yu. Denisov, A.A. Khudenko, Phys. Rev. C **79**, 054614 (2009).

[5] A.M. Lane and R.G. Thomas, Rev. Mod. Phys. **30**, 257 (1958).

[6] H.J. Mang, Phys. Rev. **119**, 1069 (1960).

[7] A. Săndulescu, Nucl. Phys. A **37**, 332 (1962).

[8] D.S. Delion and A. Săndulescu, J. Physics G **28**, 617 (2002).

[9] D.S. Delion, A. Săndulescu, and W. Greiner, Phys, Review C **69**, 044318 (2004).

[10] J. Wauters *et al.*, Z. Phys. A **342**, 277 (1992); Z. Phys. A **344**, 29 (1992); Z. Phys. A **345**, 21 (1993); Phys. Rev. C **47**, 1447 (1993); Phys. Rev. C **50**, 2768 (1994); Phys. Rev. Lett. **72**, 1329 (1994).

[11] N. Bijnens *et al.*, Phys. Rev. Lett. **75**, 4571 (1995).

[12] R.G. Allatt *et al.*, Phys. Lett. B **437**, 29 (1998).

[13] C.F. Liang *et al.*, Phys. Rev. C **49**, 2230 (1994).

[14] J.O. Rasmussen, Phys. Rev. **113**, 1593 (1959).

[15] A. Săndulescu and O. Dumitrescu, Phys. Lett. **19**, 404 (1965).

[16] A. Săndulescu and O. Dumitrescu, Phys. Lett. B **24**, 212 (1967).

[17] M.I. Cristu, O. Dumitrescu, N.I. Pyatov, and A. Săndulescu, Nucl. Phys. A **130**, 31 (1969).

[18] D.S. Delion, A. Florescu, M. Huyse, J. Wauters, P. Van Duppen, ISOLDE Collaboration, A. Insolia and R.J. Liotta, Phys.

Rev. Lett. **74**, 3939 (1995); Phys. Rev. C **54**, 1169 (1996).

[19] D.S. Delion and R.J. Liotta, Phys. Rev. C **56**, 1782 (1997).

[20] D.S. Delion and J. Suhonen, Phys. Rev. C **64**, 064302 (2001).

[21] S. Peltonen, D.S. Delion, and J. Suhonen, Phys. Rev. C **71**, 044315 (2005).

[22] C. Xu, Z.Z. Ren, Phys. Rev. C **75**, 044301 (2007).

[23] Y.Z. Wang, H.F. Zhang, J.M. Dong, G. Royer, Phys. Rev. C **79**, 014316 (2009).

[24] K.P. Santhosh, Sabina Sahadevan, Jayesh George Joseph, Nucl. Phys. A **850**, 34 (2011).

[25] O.A.P. Tavares, E.L. Medeiros, Phys. Scr. **84**, 045202 (2011).

[26] I. Silisteanu and A.I. Budaca, At. Data Nucl. Data Tables, **98**, 1096 (2012).

[27] J.O. Rasmussen and B. Segal, Phys. Rev. **103**, 1298 (1956).

[28] H.M.A. Radi, A.A. Shihab-Eldin, J.O. Rasmussen, and Luiz F. Oliveira, Phys. Rev. Lett. **41**, 1444 (1978).

[29] P.O. Fröman, Mat. Fys. Skr. Dan. Vid. Selsk. **1**, 3 (1957).

[30] H. Abele and G. Staudt, Phys. Rev. C **47**, 742 (1993).

[31] Dao T. Khoa, Phys. Rev. C **63**, 034007 (2001).

[32] R. Neu and F. Hoyler, Phys. Rev. C **46**, 208 (1992).

[33] M. Avrigeanu, A.C. Obreja, F.L. Roman, V. Avrigeanu, W. von Oertzen, At. Data Nucl. Data Tables **95**, 501 (2009).

[34] P. Mohr, G.G. Kiss, Zs. Fülöp, D. Galaviz, Gy. Gyürky, E. Somorjai, At. Data Nucl. Data Tables **99**, 651 (2013).

[35] G. Royer, Nucl. Phys. A **848**, 279 (2010).

[36] V. Yu. Denisov, and H. Ikezoe, Phys. Rev. C **72**, 064613 (2005).

[37] A. Săndulescu, A. Florescu, F. Cârstoiu, W. Greiner, J.H. Hamilton, A.V. Ramayya, and B.R.S. Babu, Phys. Rev. C **54**, 258 (1996).

[38] D.S. Delion, A. Săndulescu, S Mişicu, F. Cârstoiu, and W. Greiner, Phys. Rev. C **64**, 041303(R) (2001).

[39] D.S. Delion, A. Săndulescu, S. Mişicu, F. Cârstoiu, and W. Greiner, J. Phys. G **28**, 289 (2002).

[40] D.S. Delion, A. Săndulescu, and W. Greiner, Phys. Rev. C **68**, 041303(R) (2003).

[41] Y.A. Akovali, Nucl. Data Sheets **84**, 1 (1998).

[42] V.Yu. Denisov and A.A. Khudenko, At. Data Nucl. Data Tables **95**, 815 (2009).

[43] D.S. Delion, S. Peltonen, and J. Suhonen, Phys. Rev. C **73**, 014315 (2006).

[44] S. Peltonen, D.S. Delion, and J. Suhonen, Phys. Rev. C **78**, 034608 (2008).

[45] D.D. Ni and Z.Z. Ren, Phys. Rev. C **80**, 051303(R) (2009); Phys. Rev. C **81**, 064318 (2010); Phys. Rev. C **83**, 067302 (2011).

[46] X. Zhang, C. Xu, and Z.Z. Ren, Phys. Rev. C **84**, 044312 (2011).

[47] D.D. Ni and Z.Z. Ren, Phys. Rev. C **86**, 054608 (2012); J. Phys. Conf. Series **381**, 012055 (2012).

[48] C. Xu and Z.Z. Ren, Phys. Rev. C **73**, 041301(R) (2006); Nucl. Phys. **A 778**, 1 (2006).

[49] V. Yu. Denisov and A. A. Khudenko, Phys. Rev. C **80**, 034603 (2009).

[50] K. P. Santhosh and Jayesh George Joseph,Phys. Rev. C **86**, 024613 (2012).

[51] D.S. Delion and A. Dumitrescu, Phys. Rev. C **87**, 044314 (2013).

[52] D.E. Ward, B. G. Carlsson and S. Åberg, Phys. Rev **C 92**, 014314 (2015).

[53] W. M. Seif, M. M. Botros and A. I. Refaie, Phys. Rev. **C 92** 044302 (2015).

[54] *Evaluated Nuclear Structure Data Files* at Brookhaven National Laboratory, www.nndc.bnl.gov/ensdf/.

[55] Peter Möller *et al.*, Phys. Rev. Lett. **108**, 052501 (2012).

[56] M. Wang *et al.*, Chinese Physics C, 1603 (2012).

[57] D.S. Delion, *Theory of particle and cluster emission* (Springer-Verlag, Berlin, 2010).

[58] D.S. Delion, A. Dumitrescu, At. Data Nucl. Data Tables **101**, 1 (2015).

[59] A.A. Raduta, *Nuclear Structure with Cohent States* (Springer International Publishing, Switzerland, 2015).

[60] V.E. Viola, G.T. Seaborg, J. Inorg. Nucl. Chem. **28**, 741 (1966).

[61] Y.J. Ren and Z.Z. Ren Phys. Rev. C **85**, 044608 (2012).

[62] D.S. Delion, R.J. Liotta, and R. Wyss, Phys. Rev. Lett. **96**, 072501 (2006).

[63] C. Qi, F.R. Xu, R.J. Liotta, and R. Wyss, Phys. Rev. Lett. **103**, 072501, (2009).

[64] D. N. Poenaru, R. A. Gherghescu and Walter Greiner, J. Phys. G: Nucl. Part. Phys. **39**, 015105 (2012).

[65] A. Parkhomenko, A. Sobiczewski, Acta Phys. Polonica B **36**, 3095 (2005).

[66] A.A. Raduta and R.M. Dreizler, Nucl. Phys. A **258**, 109 (1976).

[67] A.A. Raduta, V. Ceausescu, and R.M. Dreizler, Nucl. Phys. A **272**, 11 (1976).

[68] P.O. Lipas and J. Savolainen, Nucl. Phys. A **130**, 77 (1969).

[69] P.O. Lipas, P. Haapakoski and T. Honkaranta, Phys. Scripta **13**, 339 (1976).

[70] A.A. Raduta, V. Ceausescu, A. Gheorghe, and R.M. Dreizler, Phys. Lett. B **99**, 444 (1981).

[71] A.A. Raduta, V. Ceausescu, A. Gheorghe, and R.M. Dreizler, Nucl. Phys. A **381**, 253 (1982).

[72] A.A. Raduta, R. Budaca, and Amand Faessler, Ann. Phys. (NY) **327**, 671 (2012).

[73] A. A. Raduta, D. S. Delion and N. Lo Iudice, Nucl. Phys. **A 551** (1993).

[74] G. Bertsch, J. Borysowicz, H. McManus, and W.G. Love, Nucl. Phys. A **284**, 399 (1977).

[75] G.R. Satchler and W.G. Love, Phys. Rep. **55**, 183 (1979).

[76] F. Cârstoiu and R.J. Lombard, Ann. Phys. (N.Y.) **217**, 279 (1992).

[77] P. Möller and J.R. Nix, Nucl. Phys. A **272**, 502 (1995).

[78] D. Bucurescu, N.V. Zamfir, Phys. Rev. C **87**, 054324 (2013).

[79] D. S. Delion, A. Dumitrescu, Phys. Rev. **C 92**, 021303(R) (2015).